細胞における力の発生とバランス

Cellular Force Generation and Balance

出口真次
Shinji Deguchi

機械刺激は細胞内の力（正確には，ホメオスタシスによって一定に保たれている単位面積当たりの引張力）のバランスを乱す要素として働く．この力のバランスの変化は，引張力を支えている細胞接着斑の構造に直接物理的な影響を及ぼす．その結果現れる接着斑シグナル分子の活性変化は，機械刺激による強制変形を受けにくい細胞内の位置に接着斑が再構築されると抑制されて基準レベルに戻る．このように接着斑の再構築を経て力のバランスと接着斑シグナル分子の活性化レベルが維持されるかどうかは，細胞が増殖・分化・アポトーシスのいずれの状態をとるかという根本的問題に結びつくことが示唆されている．

key words　機械刺激，メカノセンサー，ホメオスタシス

はじめに

細胞は機械刺激を感知して様々な応答を示す．この機械"刺激（英語ではしばしばmechanical stress）"という言葉の響きからは，外的な刺激（外力）を受けて初めて現れる現象というイメージを抱くかもしれない．その場合メカノセンシングとは――例えば高い血圧を受ける動脈血管の細胞など――明らかに外力を受ける器官の細胞の特殊な問題と見なされるかもしれない．しかし，じつは一見外力がなくても，分裂能を有する哺乳類細胞には（非筋Ⅱ型ミオシンに由来する）内因性の収縮力が普遍的に存在している．このとき，物理学における"力の作用・反作用の法則"から，細胞が別の細胞や細胞外マトリックスと接着している（物理的に拘束されている）限り，その構造要素には力が作用する（図1）．この細胞内部，細胞-細胞間，および細胞-細胞外マトリックス間に作用する力がおよそバランスを保って細胞群の構造が維持される（"およそ"と記したのは実際には常に変動があり，細胞群は絶えず動き続けるためである．以降の本文では，"バランス"や"合力ゼロ"の前に付けるべき"およそ"を省略する）．

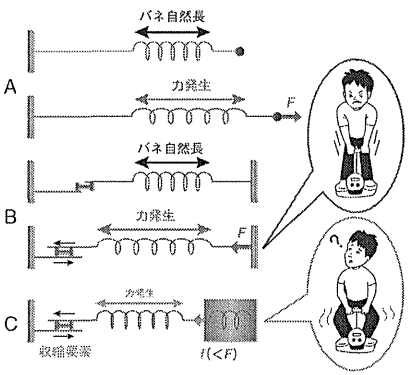

■図1　弾性要素・収縮要素および拘束物によって張力が発生する
弾性バネを外力によって引っ張っても（A），収縮要素が縮んでも（B），同じ張力Fが発生しうる（Aではバネを引っ張る力の方向に，またBではバネが拘束物を引っ張る力の方向にそれぞれ⇔を描いた）．拘束物が軟らかい場合（C）はBと同様に縮む能力があってもBほどの張力が発生しない（バネの伸びが小さい）．

さて，このように細胞群には常に力が作用していることから，機械刺激とはホメオスタシス（恒常性）によって一定に保たれている細胞内の力のバランスが一時的に乱された状態と見なせる．本稿では，細胞内で力がどのようにバランスを保っているか，またバランスを保つ機能の意義について述べる．

Ⅰ　細胞内の力のバランス

1．動きが見えないが存在する細胞内の力

一口に"力"と言っても様々なものがあるが，2つに大別できる．1つは目に見える動きを伴う力，もう1つは"細胞内の力のバランス"に関与する（一見動きのない）力である．本稿が主題とするのは後者に相当するⅡ型ミオシンが発生する張力（収縮力）である．通常"力"と言えば動きのあるダイナミックなイメージを持たれるかもしれない．例えば，細胞先導端でのアクチン重合が細胞膜を押す力が挙げられる．一方，動きを伴わない力とは地味で特殊な問題と見なされるかもしれない．しかし，この動きを伴わない力を細胞が維持するかどうかは，細胞が増殖・分化・アポトーシスのいずれをとるかという基本的問題に結びつく．

"一見動きのない"とは，力がバランスされているために見えないのである．バランスを崩せば（レーザーを用いてバランスに関与する構造物を切断するなど）動きが現れ，力の存在を確認できる[1]．あるいは細胞内にミオシン収縮力（内因性の張力）が存在することをTFM（traction force microscopy）によって確かめられる（図2）．細胞を軟らかいゲル上で培養すると，ゲルには"シワ"が寄る．TFMとはこのシワの寄り具合（ひずみ）を力学的に解析してゲル表面上の力（traction force）の分布を調べる方法である．

細胞が自力で遊走しているときはtraction forceの合力はゼロではなく，移動と同じ方向へのベクトル成分を持つ．一方，特定の方向に遊走していないspread（拡がった）しただけの状態（あるいはコンフルエント）の細胞にもtraction forceが発生しているが，それらはバランスを保っており，合力はゼロと考えてさし支えない（なおtraction forceは日本語ではしばしば"牽引力"と呼ばれる．牽引とは，レッカー車で故障車を牽引する，など特定方向に引っ張ることを含む言葉である．一方，ここで主題とする平面上に拡がった細胞が発生するtraction forceは合力ゼロであり，特定方向へ牽引しているわけではない．本稿では"引張力"と呼ぶことにする）．

2．どのようにバランスを保っているか（細胞の力学モデル）

細胞骨格の構造的役割を考慮した初期（1990年代）の細胞力学モデルにテンセグリティー（tension + integrityの造語）モデル[2]がある．このモデルではアクチンフィラメントが張力を，微小管が圧縮力をそれぞれ支え，両者が接続されて細胞全体のバランスを保つ．これは概念的なモデルにすぎないが，このような力学モデルの提示は細胞内の力のバランスと意義について議論を始めるきっかけとなった．現在では定量的な計測や解析が進み，次のことがわかっている（図2）．ま

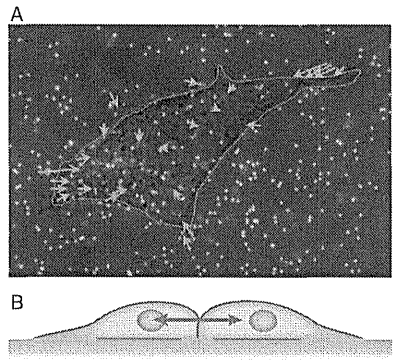

■図2　細胞内の力のバランス
A：TFMの一例．軟らかいゲルに埋め込んだ蛍光ビーズ（赤色は観察終了後に細胞を除去して無負荷となった位置，緑色は細胞がゲルに接着して引張力を作用している位置．したがって（赤色と緑色の一致する）黄色は細胞の引張力によって変形していない位置）の移動から引張力（正確には応力）を得ることができる．→は顕著なビーズの変位を強調して示したもの．細胞（蛍光の線で囲った部分）の辺縁において中心側に向かう引張力が発生する．
B：2つの細胞が接着する際の力のバランス．細胞間接着では100nNオーダーの比較的大きい張力が発生するが，その直下の細胞-マトリックス間接着における引張力は小さい．細胞辺縁での引張力は大きく（A），個々の焦点接着斑には10nNオーダーの力が作用する．

ず単一の細胞が発生する引張力の合力はゼロである．しかし，個々の焦点接着斑（focal adhesions）には10nN（ナノニュートン）のオーダーの引張力が存在している[3]．この引張力は細胞の中心側を向いており，個々の細胞で考えると合力がゼロになる．

この引張力の発生源はⅡ型ミオシン（過渡的なCa^{2+}流入を必要とせず，持続的な張力発生に関わるアイソフォームとして非筋ミオシンⅡA，非筋ミオシンⅡB，平滑筋ミオシンⅡがある）である．これはRhoキナーゼの阻害剤Y-27632を用いてミオシン調節軽鎖（myosin regulatory light chain；MRLC）のリン酸化（ミオシンが双極性のフィラメントを作り，ATP加水分解するために必要）レベルを下げたり，ブレビスタチン（blebbistatin）を用いてミオシンATP加水分解における無機リン酸の放出を抑えると引張力が消失することなどから確認される．ミオシンは単独では1pN（ピコニュートン）オーダーの力しか発生しない．しかし，焦点接着斑という高次構造を細胞質側から複数のミオシンが引っ張るため

に10nNもの大きさとなる（接着構造の単位面積当たりに換算すると，例えば筋線維芽細胞では4nN/μm^2程度[4]）．この10nNの引張力をバランスを保って維持するには，焦点接着斑を挟んで細胞の外側から綱引き状に対抗する構造物が必要である．それが細胞外マトリックスである．その他にも細胞内で核は10～100nN程度[5]，微小管は0.1nN以上[6]の圧縮力をそれぞれ支えると見積もられている．なお，微小管そのものは1pN程度の圧縮力で容易に変形してしまうが，細胞質内のアクチンメッシュワークと共存下では曲げに対する剛性が増すために100倍以上もの圧縮力が支えられるのである．

以上は，単一の細胞における力のバランスについてであったが，細胞群でも力のバランスが存在する．腎上皮MDCK細胞同士が接着しているとき，細胞間には100nNオーダーの張力が発生している[7]（図2）．この力は細胞の形態や細胞間接着の長さが変わってもおよそ不変であると報告されている．また，このように細胞間に大きな張力が存在していても，細胞間接着の下側にある細胞-細胞外マトリックスの境界面にはほとんど引張力が発生していない．つまりコンフルエントの細胞群において細胞同士は互いを比較的大きな張力で引っ張り合いながらマトリックスに対しては小さい引張力のみ作用している．

Ⅱ 力のバランスの意義

1．焦点接着斑の再配置と同期する一過性の応答

細胞は機械刺激に応答して自身の構造を変化させる．例えば，内皮細胞に（拍動による周期的血管拡張を模擬して）"繰り返し伸展刺激"を負荷すると，伸展方向とは垂直の方向に配向・伸張する（図3上）．入力としての機械刺激が，生化学的変化（例えばCa^{2+}流入や何らかのシグナル分子との結合親和性の変化など）へと変換する分子はメカノセンサーと呼ばれる．これまでのメカノバイオロジー研究ではメカノセンサーの同定に主眼が置かれていた．例えば，焦点接着斑に存在するp130Casは外力によって強制的にコンフォメーションが変わり，与えた引張ひずみに比例した分だけSrcによるリン酸化を受けるメカノセンサーであることが示されている[8]．

"力のバランス"の意義や細胞の機械刺激応答はメカノセンサー（およびその下流のシグナル分子）に関する知識だけでは必ずしも理解できない．まず，形態変化には焦点接着斑の再構築が必要である．そこで例えば，焦点接着斑タンパク質のFAKや下流シグナルのJNKなどMAPキナーゼ

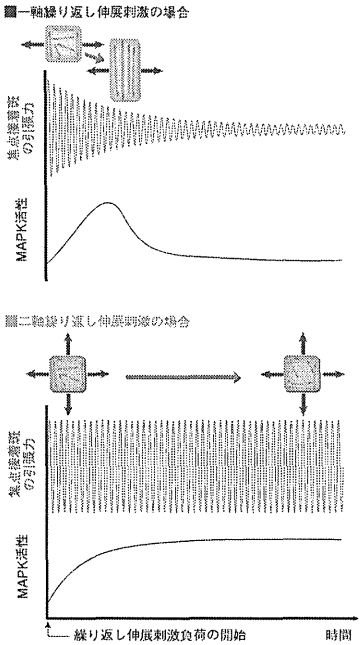

図3 焦点接着斑の再構築に同期した一過性のシグナル応答
単軸方向（↔）に繰り返し伸展刺激を負荷すると，およそ30分程度で伸展とは垂直方向に焦点接着斑（緑色）が配向する（オレンジ色は非筋Ⅱ型ミオシンを含むアクチンバンドルを示す）．そのため焦点接着斑は伸展刺激によって自らが受ける強制変形（および引張力の変動）が抑制される（赤線波形の減衰）．この焦点接着斑の再構築に同期してJNKを含むMAPKの活性化が抑制される．二軸方向繰り返し伸展刺激負荷時は，強制変形を避けられる方向がなく，焦点接着斑，ひいては細胞は特定の方向に配向しない．それに伴いMAPKの活性変化も持続する．
Kaunas R & Deguchi S: Cell Mol Bioeng (2011) 4: 182-191より改変．

（MAPK）に注目すると，それらは繰り返し伸展刺激を与えると一過性にリン酸化レベルを変化させる[9)~11)]．この"一過性の応答"は細胞の構造変化（具体的には焦点接着斑が機械刺激による強制変形を受けにくい細胞内の位置への再構築，すなわち伸展方向とは垂直の方向への細胞配向）と同期しており，再構築を終えると基準レベルに戻る．その後，引き続き細胞に繰り返し伸展刺激を与えても，それ以上変化が

起こらない．つまり入力としての継続的外力負荷とメカノセンサー下流のシグナル分子活性の間には相関がない．さらに，二軸方向への繰り返し伸展刺激負荷[11]，あるいは方向性のない流れずり応力（disturbed flow）負荷[9), 10)]のもとでは細胞は特定の方向へ配向しない（図3下）．これらの物理環境では焦点接着斑が"機械刺激による強制変形"を避けられず，このときFAKやMAPKの活性化は一過性に沈静することなく持続する．

このことは，機械刺激への適応（接着構造が強制変形を受けにくいように再構築すること，すなわち機械刺激の方向とは垂直に細胞が配向すること）を達成したとして満足感を抱き（物理の言葉で言えば，自由エネルギーが極小値を持ち），細胞接着由来のシグナル分子の活性を基準レベルに戻し，かつ（見かけの）応答を終える機構が存在することを意味する．したがって単なる力（従来的なメカノセンサーが感知できるもの）ではなく，細胞にとって（上記の満足感を抱かせる）"適応に適う"力を識別し，そこからの"ずれ"を補正する負のフィードバック（作用）が細胞内に存在することを示唆する．このように本問題の解明にはメカノセンサーという一要素の概念を超えて，分子と物理の複合的知識と考察に基づく細胞挙動のシステム的理解が求められる．

2．引張力のホメオスタシス

外力負荷を除く，すなわち静置培養の状態に戻すと細胞は元の形態に戻る．つまり図3の構造変化は（分化やアポトーシスを導くしきい値[4), 12), 13)]を超えない限り）可逆的である．このことから細胞は何らかの力学量が関与した恒常性（ホメオスタシス）を保つ機構を有していると考えられる．"構造変化が止む＝応答を終えること"を"ホメオスタシスの基準状態に移った（戻った）"と捉える視点がポイントである．

このホメオスタシスにおける恒常値，すなわち細胞にとっての"適応に適う力"は何か？繰り返し進展刺激を与えると垂直方向に伸張した形態へと変化して適応応答を終える（図3上）．適応の前後で（見た目の）細胞形態が変わるため，見た目の形態（に関わる力学的な量）は恒常値として制御される対象ではない．したがって形態という"見た目"ではなく，細胞の"内"に"適応に適うように"制御される物理対象があり，形態変化を利用するなどして（機械刺激によって引き起こされる）外乱を抑制すると考えられる．初めに述べたとおり，細胞内には無負荷静置培養下（つまり恒常状態）においても，ミオシン収縮（収縮と言っても見た目の長さが縮むわけではないために等尺性収縮と呼ばれる）による引張力が発生している．

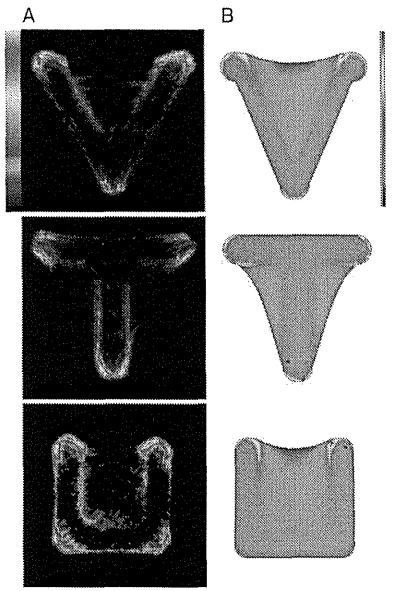

図4 焦点接着斑は細胞内で力学的負荷がかかりやすい場所に形成される
A：V，T，U字型のマイクロパターン上にそれぞれ培養した単一細胞のビンキュリンの発生位置．
B：細胞内で力がかかりやすい場所を調べた構造解析結果．焦点接着斑（ビンキュリンで標識）の局在と高い相関があることから，正の作用（力が強い場所ほど接着が促進される）が示唆される．
Deguchi S, et al: Cytoskeleton (2011) 68: 639-651より改変．

筆者らはこの"見た目"には現れないものの，常に細胞に内在する引張力（正確には焦点接着斑に作用する単位面積当たりの引張力）がホメオスタシスの調節対象（上記の"適応に適う力"に相当）であることを示す結果を得ている[11]．

ホメオスタシスの実現には正および負の両作用が必要であるが，本稿では正の作用のみ説明する．機械刺激（負の作用を引き起こす）が不在の静置培養時を考える[14), 15)]．図4Aはそれぞれ（細胞のサイズと同程度の）微小なアルファベット文字V，T，U字型を持つマイクロパターン上に培養した単一の細胞を示す．このとき焦点接着斑（ビンキュリンを蛍光標識）は必ず細胞内の特定の位置に現れる．一方，図4Bは（単

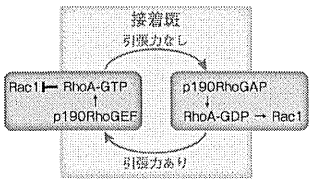

■図5 引張力の有無に依存した接着斑機能モデル
発達した接着斑ではp190RhoGEFがFAKに結合してリン酸化され，RhoAを局所的に活性化する[16]．その結果，MRLCのリン酸化を経てさらに引張力を高め，接着斑を成熟させるという正の作用が働くと考えられる．

位面積当たりの）引張力の空間分布を解析した結果を示しており，ビンキュリンの局在と高い相関があることがわかる．つまり"引張力の大きい場所ほど細胞接着が発達する"という正の作用の存在を強く示唆している．焦点接着斑におけるこの正の分子活性経路として，他のグループおよび筆者らの結果を併せて"引張力→FAK・Src→p190RhoGEF→RhoA→Rhoキナーゼ→MRLC→引張力→……繰り返し"を想定して研究を進めている．

なお，（インテグリンと細胞外マトリックスとの結合だけが起こり）引張力が存在しない場合にはp190RhoGEFの代わりにp190RhoGAPの働きが支配的となってRhoAの活性化を抑える[16]．つまり細胞接着の複合構造に引張力が作用するか否かで異なるRhoAの調節因子が活性化されるという考えが提示されている（図5）．細胞間接着でも同様にp190RhoGAPはカドヘリンのホモフィリックな結合によって一時的に活性化されてRhoAを不活化するが，成熟した細胞間接着はむしろ（RhoAが活性化されて）基準レベルの張力が存在すれば安定化される[17]．このように接着構造は最初の（細胞-マトリックス間あるいは細胞-細胞間）結合ではRhoAを不活化して引張力を発生させず（逆にRac1の活性化を通して仮足の形成を促し）より柔軟性を持たせて移動しやすいようにする．そして（図4のマイクロパターンの頂点部分に位置取りするなど）いったん持続的に張力がかかりやすい状態になると，正の作用のために接着が強化されると考えられる．

なお，筆者らは当ホメオスタシスの負の作用を担うことができるのは非筋Ⅱ型ミオシンを含む複合体だけと考え，その分子メカニズムの研究を進めている[11]．このミオシン複合体は単に力を感知するメカノセンサーとしてだけではなく，（上記の）"適応に適う引張力"を得るまで自己再構築を行うメカノコントローラーの役割を果たすと考えられる．

おわりに

最初にこれが特殊な問題でないと記した根拠の1つは，細胞分裂が可能な細胞種に広く発現する非筋Ⅱ型ミオシンが主役を演じることである．細胞が接着するマトリックスが軟らかすぎるとき，あるいはマイクロパターンを用いて接着面積を制限し細胞が拡がることができないとき，非筋Ⅱ型ミオシンは（ホメオスタシスを保障する）基準レベルの引張力を（物理的に）発生することができない（図1C）．このとき内皮細胞ではアポトーシス[9]，上皮細胞では一次繊毛の形成[15]，間葉系幹細胞では引張力の大きさに応じて特定の細胞種への分化[13]がそれぞれ導かれることが確認されている．一方，引張力が基準レベルよりも大きいときも間葉系幹細胞では特定の細胞種へと分化し[13]，また，筋線維芽細胞では支配的なアクチンのアイソフォームを変えてより大きい引張力（13nN/μm^2）を恒常値とするフェノタイプに移る[4]．

機械刺激とは，このように細胞の増殖・分化・アポトーシスへ至る条件を左右する非筋Ⅱ型ミオシン依存細胞内張力バランスを乱すものと見なせる．接着構造が機械刺激に晒され続けざるをえない二軸繰り返し伸展刺激やdisturbed flowの物理環境（図3下）において持続的に活性化されるMAPKは炎症を誘発する因子でもある．慢性炎症が原因とされる動脈硬化症が血管分岐部などdisturbed flow領域で局所的に起こることから，免疫応答の関与以前に，ここで述べた（何らかの機能不全により細胞接着の再構築が不可能な細胞の）問題の炎症慢性化への関与が示唆される[9)~11)]．とりわけここで述べた引張力のホメオスタシスと細胞生理・病理の関係は細胞生物学の従来的知識を超えた新しい概念であるために，さらに緻密で多面的な検証研究が必要である．

謝辞 松井 翼博士をはじめ共同研究者に感謝します．

PROFILE 出口真次
■ 東北大学大学院工学研究科 准教授
■ E-mail：deguchi@bml.mech.tohoku.ac.jp
■ 趣味：子どもと遊ぶ・読書（サイエンス・医学）・スポーツ観戦
2001年名古屋大学大学院工学研究科修士課程修了，2004年東北大学大学院工学研究科博士課程修了（博士（工学）），岡山大学大学院自然科学研究科助教を経て，2007年より東北大学准教授．

文献
1) Rajfur Z, et al: Nat Cell Biol (2002) 4: 286-293
2) Wang N, et al: Science (1993) 260: 1124-1127
3) Deguchi S, et al: J Biomech (2006) 39: 2603-2610
4) Goffin JM, et al: J Cell Biol (2006) 172: 259-268
5) Deguchi S, et al: J Mech Behav Biomed Mater (2009) 2: 173-185
6) Brangwynne CP, et al: J Cell Biol (2006) 173: 733-741
7) Maruthamuthu V, et al: Proc Natl Acad Sci USA (2011) 108: 4708-4713
8) Sawada Y, et al: Cell (2006) 127: 1015-1026
9) Chien S: Am J Physiol Heart Circ Physiol (2007) 292: H1209-H1224
10) Hahn C & Schwartz MA: Nat Rev Mol Cell Biol (2009) 10: 53-62
11) Kaunas R & Deguchi S: Cell Mol Bioeng (2011) 4: 182-191
12) Chen CS, et al: (1997) 276: 1425-1428
13) Engler AJ, et al: Cell (2006) 126: 677-689
14) Théry M, et al: Cell Motil Cytoskeleton (2006) 63: 341-355
15) Deguchi S, et al: Cytoskeleton (2011) 68: 639-651
16) Tomar A & Schlaepfer DD: Curr Opin Cell Biol (2009) 21: 676-683
17) Noren NK, et al: J Biol Chem (2003) 278: 13615-13618
18) Pitaval A, et al: J Cell Biol (2010) 191: 303-312

Lab on a Chip

Dynamic Article Links

Cite this: *Lab Chip*, 2012, **12**, 4336–4343

www.rsc.org/loc

PAPER

Separation of cancer cells from a red blood cell suspension using inertial force

Tatsuya Tanaka,[a] Takuji Ishikawa,*[a] Keiko Numayama-Tsuruta,[b] Yohsuke Imai,[a] Hironori Ueno,[c] Noriaki Matsuki[d] and Takami Yamaguchi[b]

Received 13th April 2012, Accepted 11th July 2012
DOI: 10.1039/c2lc40354d

The circulating tumor cell (CTC) test has recently become popular for evaluating prognosis and treatment efficacy in cancer patients. The accuracy of the test is strongly dependent on the precision of the cancer cell separation. In this study, we developed a multistage microfluidic device to separate cancer cells from a red blood cell (RBC) suspension using inertial migration forces. The device was able to effectively remove RBCs up to the 1% hematocrit (Hct) condition with a throughput of 565 μL min^{-1}. The collection efficiency of cancer cells from a RBC suspension was about 85%, and the enrichment of cancer cells was about 120-fold. Further improvements can be easily achieved by parallelizing the device. These results illustrate that the separation of cancer cells from RBCs is possible using only inertial migration forces, thus paving the way for the development of a novel microfluidic device for future CTC tests.

1. Introduction

Cancer remains one of the most deadly diseases in many developed countries. Because 90% of all cancer-related deaths occur due to cancer metastasis,[30] it is crucial to accurately detect the metastasis or recurrence of cancer at an early stage. Recently, the circulating tumor cell (CTC) test has become popular for evaluating prognosis and treatment efficacy in cancer patients.[4,8,9] In such tests, the condition of a patient is evaluated by counting the number of cancer cells in a peripheral blood sample; thus, the identification or separation of cancer cells from other blood cells is necessary. The accuracy of the CTC test is strongly dependent on the precision of cell identification or separation. Because conventional methods require several biochemical techniques for identification, they have serious drawbacks, such as high costs, long process times, and complex procedures.

Several techniques have been developed for separating cells, such as fluorescence-activated cell sorting (FACS), magnetic sorting, and dielectrophoresis.[11,24] Because these separation techniques require that the cells be labeled, they have problems of high cost, a complex preparation procedure, and the need for a large space to house the separation apparatus.

[a]*Dept. Bioengineering and Robotics, Graduate School of Engineering, Tohoku University, 6-6-01 Aoba, Aramaki, Aoba-ku, Sendai, 980-8579, Japan. E-mail: ishikawa@pfsl.mech.tohoku.ac.jp; Fax: +81-22-795-6959; Tel: +81-22-795-4009*
[b]*Dept. Biomedical Engineering, Graduate School of Biomedical Engineering, Tohoku University, 6-6-01 Aoba, Aramaki, Aoba-ku, Sendai 980-8579, Japan*
[c]*International Advanced Research and Education Organization, Tohoku University, 6-6-01 Aoba, Aramaki, Aoba-ku, Sendai, 980-8579, Japan*
[d]*Dept. Biomedical Engineering, Graduate School of Engineering, Okayama University of Science, Ridai-cho, Okayama 700-0005, Japan*

With the recent rapid progress of micro-fabricating technologies, passive microfluidic devices, which use only hydrodynamic forces for separation, have received much attention because of their favorable properties, such as low cost, simple procedure, and the small amount of space needed to house the apparatus. Separation based on the inertial migration of particles is one of these techniques,[7] which is typically applied to the separation of rigid spheres with different sizes.[18] Because the throughput of this separation method is very high, we think it may be suitable for CTC tests dealing with large numbers of cells.

Recently, some groups have succeeded in detecting or separating different cell types using an inertial migration effect. Kuntaegowdanahalli *et al.*[14] developed a five-loop Archimedean spiral microchannel and separated SH-SY5Y neuroblastoma cells (~15 μm in diameter) from C6 rat glioma cells (~6 μm in diameter).[2] They were able to perform the separation using a combination of inertial migration force and the Dean force generated by the centrifugal effect. Hur *et al.* demonstrated three-dimensional focusing of cells through channels using inertial migration forces.[12] Because this alignment could prevent overlapping and out-of-focus cells, their device allowed RBCs and leukocytes to be counted using image analysis. Carlo and coworkers applied the inertial migration effect to isolate platelets or bacteria from other blood cells in a diluted suspension, and succeeded in enriching the relative number of platelets and bacteria.[5,6,17]

Most recently, Bhagat *et al.* developed a microfluidic device that utilizes a pinched effect and inertial migration effect for separating cancer cells from a diluted whole blood sample.[4] It consisted of a cell-focusing region and a rare-cell pinching region. In the cell-focusing region, all cells migrated and aligned near the sidewalls due to inertial migration forces. The rare-cell pinching region had a geometry that contained contraction-expansion subunits. Since the width of the contraction channel was set at a smaller size than the cancer cell, cancer cells underwent squeezing forces in this section, and the center of inertia of these larger cells was aligned along the center of the microchannel. Although the device showed high separation efficiency and separation purity, limitations in throughput and the risk of clogging at the narrow contraction region require improvement. To avoid clogging while maintaining high throughput, we considered developing a microfluidic device to separate cancer cells from blood using only an inertial migration effect.

In a previous study,[28] we investigated the applicability of inertial migration forces to separate cancer cells from a concentrated suspension of RBCs. The experimental results revealed that the inertial migration of cancer cells occurred up to about a 10% Hct condition. Although the developed device was able to collect cancer cells from an RBC suspension, it did not achieve high enrichment of cancer cells. Thus, in the current study, we sought to develop a microfluidic device to separate cancer cells from an RBC suspension with high collection efficiency and enrichment. Although the separation of leukocytes is also important in considering applications to CTC tests, the separation of cancer cells from RBCs should be investigated first, given that RBCs make up most of blood constituents and no former studies have succeeded using only inertial forces.

2. Materials and methods

2.1 Experimental setup

The experimental apparatus consisted primarily of an inverted microscope (IX71, Olympus, Tokyo, Japan) and a high-speed camera (Phantom v7.1; Vision Research, Wayne, NJ). A microchannel was placed on the stage, and the sample was injected using a syringe pump (Fusion 200; Chemyx Inc., Stanford, TX). Images of rigid spheres and cells were taken with the high-speed camera and recorded on a desktop PC.

A schematic of the microchannel is shown in Fig. 1(a). The device had a cascade geometry of stenosed channels and expansions with multiple bifurcations. The height of the channel was 160 μm. The flow rate ratio between the channels leading to the RBC-outlet and cancer-outlet was set at each bifurcation point as follows: approximately 1 : 1 at B1, 1 : 1.2 at B2, 1 : 1.4 at B3, and 1 : 0.5 at B4. The flow ratios were determined so as to lead only RBCs to the RBC-outlet and only cancer cells to the cancer-outlet, which was controlled by adding the appropriate channel resistances.[1] The total flow rate ratio between RBC-outlet and cancer-outlet was about 8.1 : 1.

Fig. 1(b) shows the principle of the separation method used. The microfluidic device uses the inertial migration of cancer cells in the stenosed channels and the increase in the cell-free layer of RBCs at the multiple bifurcations. First, cell-free layers were formed after the first stenosed channel [Fig. 1(b)(i)]. Cancer cells then migrated towards their equilibrium positions after the second stenosed channel [Fig. 1(b)(ii)], where the equilibrium positions existed at approximately $0.6W$ (W: the half width of the channel) away from the channel center.[2] The first bifurcation (B1) split the main flow into two [Fig. 1(b)(iii)], and then cancer cells migrated to their equilibrium position after the third stenosed channel [Fig. 1(b)(iv)]. In this channel, cancer cells migrated towards only one side of the channel, because the equilibrium position existed $0.6W$ away from the center. At the second bifurcation (B2), an RBC suspension without cancer cells was extracted towards the RBC-outlet and the cell-free layer thickness in the main channel was increased significantly. These successive operations resulted in a reduction in the overlap between cancer cells and RBCs. Finally, cancer cells and RBCs were completely separated at B4 [Fig. 1(b)(v)]; only cancer cells flowed into the cancer-outlet.

The microchannel was fabricated by standard soft lithography with a protocol similar to our previous study.[15] Briefly, a mold for the channel was fabricated on a silicon wafer with a negative photoresist (SU-8 3050; Kayaku MicroChem, Tokyo, Japan). Polydimethylsiloxane (PDMS) (Silpot 184; Dow Corning, Midland, MI) was prepared by mixing the base compound and curing agent at a weight ratio of 10 : 1. After removing bubbles created during mixing, the mixture was poured on the master mold and cured by baking for about 30 min at 90 °C. The PDMS was peeled from the master, and the fluidic ports used as the inlet and the outlets were created with a punch. To prevent fluid leakage from the gap between the PDMS and glass slide, an oxygen plasma treatment was applied to irreversibly bind the PDMS and glass.

2.2 Materials

The poorly differentiated human breast cancer cell line MDA-MB-231 was used for the present study. The average diameter of the cells was about 15 μm. Cells were cultured in a 25 cm^2 tissue culture flask and maintained in RPMI 1640 (Invitrogen Corp., Carlsbad, CA) with 10% fetal bovine serum (FBS; Thermo Fisher Scientific Inc., Waltham, MA) and 1× antibiotic-antimycotic (Invitrogen) at 37 °C in a humidified atmosphere containing 5% v/v CO_2.[13] In each experiment, cells were grown to 80–90% confluence, and harvested from the tissue culture flasks by adding 0.25% trypsin-EDTA (Invitrogen) and dissociated. The cells were then used in the experiments after washing twice with Dulbecco's phosphate-buffered saline [D-PBS(-)] (Invitrogen).

RBCs were taken from healthy 25- and 26-year-old male and 25-year-old female volunteers and centrifuged to separate the RBCs and other constituents. The RBCs were then preserved in normal saline at 4 °C and resuspended in 5% Dextran 40 (DEX40), in which DEX40 (low density Dextran L 10% w/v in lactated Ringer's solution; Otsuka Pharmaceutical Co. Ltd., Tokyo, Japan) was diluted with the same volume of lactated Ringer's solution (Otsuka Pharmaceutical) prior to each experiment. All procedures were carried out in compliance with the guidelines of the Clinical Investigation Ethics Committee at Tohoku University.

Five types of fluid samples were used:

(a) To observe RBC motion, RBCs alone were suspended in 5% DEX40. The Hct ranged from 0.1% to 10%. The density and viscosity of 5% DEX40 at 25 °C were 1.01 × 10^3 kg m^{-3} and 1.99 × 10^{-3} Pa s, respectively.

(b) In rigid sphere collection experiments, only rigid spheres of 15 μm diameter (15 μm Polymer Microsphere Suspension; Thermo Fisher Scientific Inc.) were suspended in 5% DEX40. The concentration of rigid spheres was set at 1 × 10^4 particles mL^{-1}.

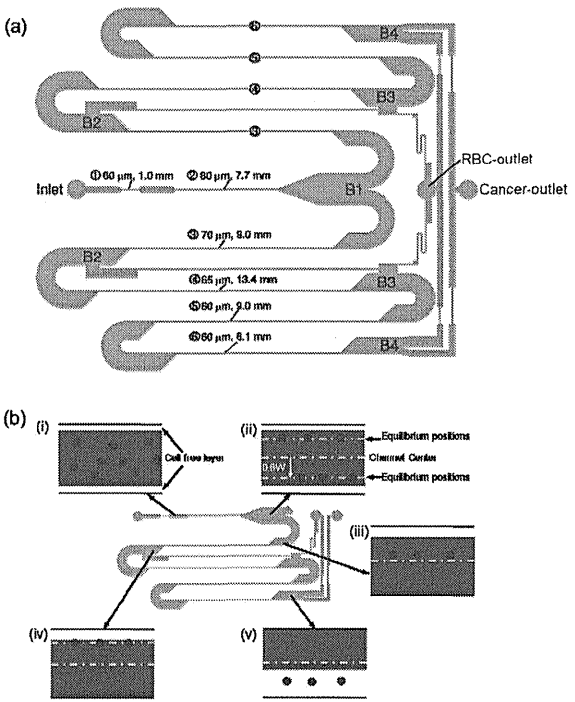

Fig. 1 Schematic of the multistage microchannel system: (a) geometry (width and length) of the device and (b) separation principle of cancer cells from an RBC suspension.

(c) In cancer cell collection experiments, only cancer cells (MDA-MB-231) were suspended in 5% DEX40. The concentration of cancer cells was set at 1×10^4 cells mL^{-1}.

(d) In experiments separating rigid spheres from RBCs, a suspension of 15 μm rigid spheres and RBCs in 5% DEX40 was prepared. The Hct of RBCs was set at 1%, and the ratio of rigid spheres to RBCs was set in the range of 0.03 to 0.1.

(e)In experiments separating cancer cells from RBCs, a suspension of cancer cells and RBCs in 5% DEX40 was prepared. The Hct of RBCs was again set at 1%, and the ratio of cancer cells to RBCs was set in the range of 0.03 to 0.1.

2.3 Experimental procedures

In experiments with fluid (a), a suspension of only RBCs, the total infusion volume was set at 10 mL. Samples were collected from each outlet and the concentration of RBCs in each sample was measured using a cell counter (Vi-CELL XR Cell Viability Analyzer; Beckman Coulter Inc., Brea, CA). We define the unsuccessful collecting ratio of RBCs from the cancer-outlet, α, as:

$$\alpha = \frac{n_{\text{c-out}}}{\lambda\, n_{\text{R-out}} + n_{\text{c-out}}} \times 100 \quad [\%] \tag{1}$$

where $n_{\text{R-out}}$ is the number density of particles in a sample collected from the RBC-outlet and $n_{\text{c-out}}$ is that from the cancer-outlet. λ is the flow rate ratio between the RBC-outlet and the cancer-outlet, which was 8.1 in this study.

In experiments with fluids (b) and (c), suspensions of only rigid spheres or cancer cells, respectively, particle motion was recorded at bifurcation B4 with a high-speed camera. The images were analyzed and the number of particles flowing into the cancer-outlet or RBC-outlet was counted. The collection efficiency of particles from the cancer-outlet was defined by the ratio of particles flowing into the cancer-outlet to the total particle number. We counted more than 200 particles to calculate the collection efficiency in each experiment.

In experiments with fluids (d) and (e), rigid spheres or cancer cells in an RBC suspension, respectively, it was difficult to observe individual particles and to count the number of particles using image analysis. We therefore used a flow cytometer (JSAN; Bay Bioscience, Hyogo, Japan) to measure the number density of rigid spheres or cancer cells. The number density of rigid spheres in an RBC suspension was counted by measuring the side scatter (SSC) of the particles. To measure the number density of cancer cells in an RBC suspension, cancer cells were labeled with nuclear staining. The labeling protocol was similar to that in our previous study.[28] Briefly, cells were separated from the 5% DEX40 solution by centrifugation. Then, 2 μL of 100-fold diluted DRAQ5 {1,5-bis[(2-(di-methylamino)ethyl) amino]-4, 8-dihydroxyanthracene-9, 10-dione} (Cell Signaling Technology Inc., Danvers, MA) solution was added to the sample, as was 98 μL of PBS, before mixing gently and incubating for 20 min at 4 °C. The sample was washed twice with fresh PBS to remove excess dye. The number density of labeled cancer cells in each sample was determined by measuring the fluorescence intensity of cells. A control test was also performed using non-labeled samples.

The collection efficiency and enrichment of rigid spheres (or cancer cells) were calculated using the following equations:

$$\text{Collection efficiency} = \frac{n_{\text{c-out}} R_{\text{c-out}}}{\lambda\, n_{\text{R-out}} R_{\text{R-out}} + n_{\text{c-out}} R_{\text{c-out}}} \times 100 \quad [\%] \tag{2}$$

$$\text{Enrichment} = \frac{R_{\text{c-out}}}{R_{\text{original}}} \tag{3}$$

where $n_{\text{R-out}}$ is the number density of particles, including rigid spheres (or cancer cells) and RBCs, collected from the RBC-outlet, $n_{\text{c-out}}$ is that from the cancer-outlet, $R_{\text{R-out}}$ is the ratio of rigid spheres (or cancer cells) to RBCs in a sample collected from the RBC-outlet, $R_{\text{c-out}}$ is that in a sample collected from the cancer-outlet, and R_{original} is that in the original sample.

In all of these experiments, the inlet flow rate was set as 565 μL min^{-1}.

3. Results

3.1 Effect of Hct on RBC motion

To achieve high separation purity, it is important to prevent the unsuccessful collection of RBCs from the cancer-outlet. In this section, we use a suspension of only RBCs [fluid (a)] to investigate the effect of Hct on RBC motion. Fig. 2(a) shows the distribution of RBCs at five observation areas under the 1% Hct condition. After the first stenosed channel, a clear cell-free layer developed near the sidewalls. The thickness of the cell-free layer was increased by the repeated bifurcations. Eventually, at the final bifurcation (B4), most of the RBCs were collected from the RBC-outlet.

Samples were collected from the two outlets and the number density of RBCs in each sample was measured. The unsuccessful collecting ratio of RBCs from the cancer-outlet, α, was then calculated using eqn (1). Fig. 2(b) shows the effect of Hct on α. We see that α increased as Hct increased. This is primarily because the thickness of the cell-free layer decreases as Hct is increased. A similar tendency was also found in our previous study,[10] in which a decrease in the cell-free layer thickness was explained by the diffusion of RBCs due to cell–cell interactions. The results of Fig. 2(b) indicate that the device was able to effectively remove RBCs up to the 1% Hct condition.

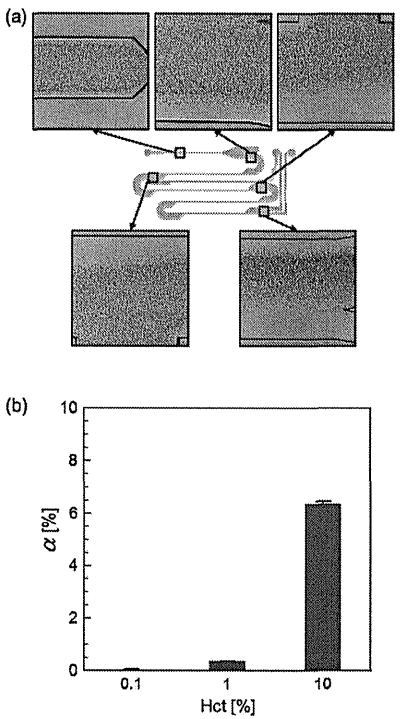

Fig. 2 Effect of hematocrit (Hct) on red blood cell (RBC) motion: (a) distribution of RBCs at five observation areas under a 1% Hct condition; (b) the effect of Hct on α ; error bars indicate the standard deviation.

3.2 Trajectories of rigid spheres and cancer cells

Next, we investigated the collection efficiency of rigid spheres (15 μm diameter) or cancer cells using a suspension of only rigid spheres or cancer cells [fluid (b) or (c), respectively]. Fig. 3(a) shows the behavior of cancer cells at the four bifurcation areas. At each area, cancer cells were aligned along the same line and most of the cancer cells were collected from the cancer-outlet. The rigid spheres showed similar tendencies to the cancer cells (data not shown).

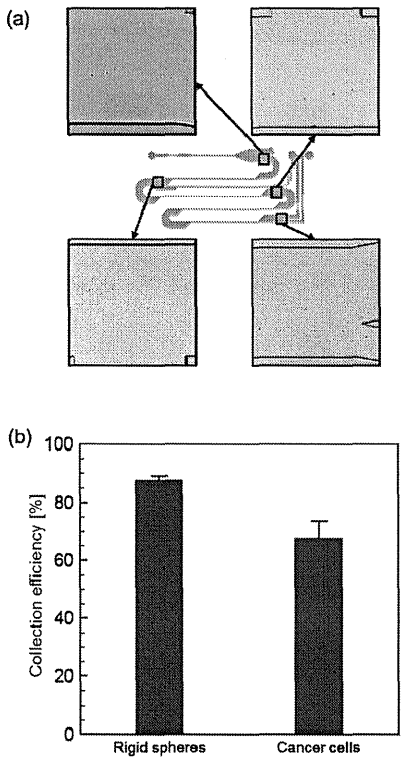

Fig. 3 Separation of rigid spheres and cancer cells: (a) the behavior of cancer cells at four bifurcation areas; (b) collection efficiency of rigid spheres and cancer cells. Error bars indicate the standard deviation.

The collection efficiency of rigid spheres or cancer cells was calculated as explained in section 2.3, and the results are shown in Fig. 3(b). The collection efficiencies of rigid spheres and cancer cells were about 88 ± 2% and 68 ± 6%, respectively. The collection efficiency of cancer cells was lower than that of rigid spheres. This was likely because the cancer cells showed individual differences in size and shape. The size distribution of MDA-MB-231 was reported in our previous study;[28] the average cell diameter was approximately 15 μm, with a standard deviation of about 4.3 μm. Based on previous studies,[19,20,25] equilibrium positions shift towards the channel center as the particle size becomes larger. Thus, in the present study, the equilibrium positions of larger cells shifted towards the channel center, and some of these cells might have flown into the RBC-outlet at bifurcation B2. As a result, some cancer cells were not collected from the cancer-outlet, and the collection efficiency was decreased as compared with the rigid sphere case. These results indicate that the distribution of cell size is an important factor in separating cancer cells by inertial migration.

3.3 Separation of rigid spheres and cancer cells from an RBC suspension

Finally, the separation of rigid spheres or cancer cells from an RBC suspension was examined using fluids (d) and (e), respectively. The Hct of the RBC suspension was set at 1%, because the unsuccessful collecting ratio of RBCs, α, was small [*cf.* Fig. 2(b)]. Since the ratio of rigid spheres or cancer cells to RBCs was set in the range of 0.03–0.1%, the two-body interactions between two rigid spheres or two cancer cells would be expected to be negligible.

Fig. 4(a) (bottom-left) shows the behavior of rigid spheres and RBCs at the final bifurcation (B4). Most of the RBCs, shown by gray dots, were collected from the RBC-outlet, while most of the rigid spheres, shown by black dots, were collected from the cancer-outlet. Fig. 4(a) (bottom-right) shows the behavior of cancer cells and RBCs at B4. We again see that most cancer cells, shown by white dots, were collected from the cancer-outlet. These results illustrate that the device could separate rigid spheres and cancer cells from RBCs.

The fluorescence intensities of samples collected from the RBC-outlet and the cancer-outlet were assessed by flow cytometry and the results of a suspension of cancer cells and RBCs [fluid (e)] are shown in Fig. 4(b). The graph is divided into four regions; the lower left region indicates non-labeled cells (*i.e.*, RBCs) and the upper right region indicates labeled cells (*i.e.*, cancer cells). We see that the sample taken from the cancer-outlet had a considerably larger number of cancer cells than that taken from the RBC-outlet.

The channel length required for focusing to equilibrium positions is given by:[7]

$$L_m = \frac{4\pi\mu W^2}{\rho U d^2 f_L} \quad (4)$$

where μ is the viscosity, ρ is the density, U is the average velocity, d is the particle diameter, and f_L is the geometric coefficient. In the first stenosed channel before bifurcation B1, for example, W is 40 μm and f_L is 0.05.[7] By assuming that the diameter of cancer cells is 15 μm, L_m can be calculated as 4.6mm, which is shorter than the channel length of 7.7 mm. Thus, most of the cancer cells can migrate to the equilibrium positions. RBCs, on the other hand, have diameters of about 8 μm. L_m for RBCs is about 16.2 mm, which is longer than the channel length. Thus, most of RBCs may not have enough time to migrate to the equilibrium positions. Eqn (4) can nicely explain the present experimental results.

As explained in section 2.3, the collection efficiency [eqn (2)] can be calculated by the ratio of cancer cells (or rigid spheres) to RBCs as well as the number density of all particles. Fig. 4(c) and (d) show the collection efficiency of rigid spheres and cancer cells, respectively. The collection efficiency of rigid spheres with 1% Hct was about 86 ± 9%, which was not different from that without RBCs (0% Hct). In the case of cancer cells, on the other hand, the collection efficiency with 1% Hct was about 85 ± 7%,

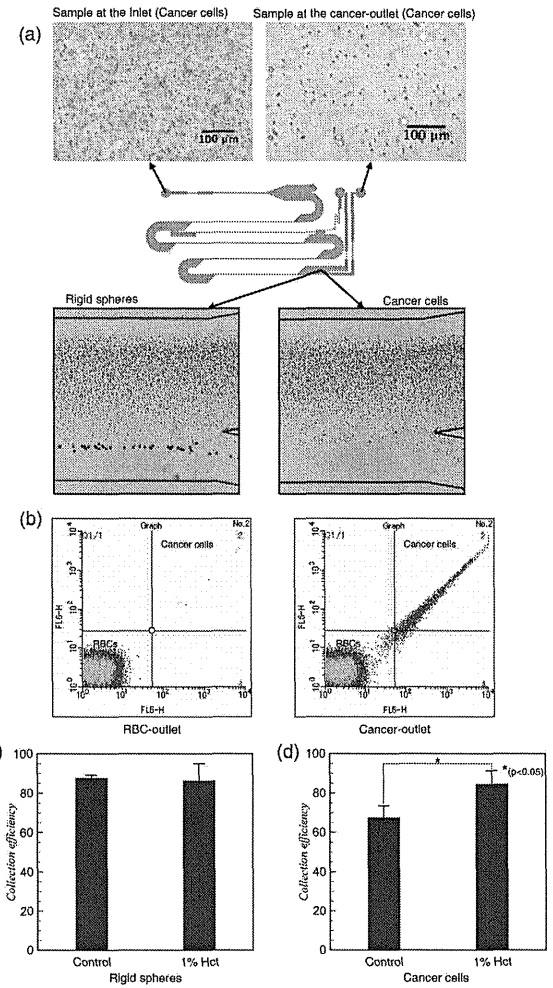

Fig. 4 Separation of cancer cells and rigid spheres from RBCs: (a) a suspension of cancer cells and RBCs at the inlet (top-left), at the final bifurcation B4 (bottom-right), and at the cancer-outlet (top-right). Bottom-left image is a suspension of rigid spheres and RBCs at B4; (b) fluorescence intensity of samples collected from the RBC-outlet and cancer-outlet in the case of a suspension of cancer cells and RBCs; (c, d) the collection efficiency of rigid spheres and cancer cells. The control indicates the collection efficiency without RBCs, and error bars indicate the standard deviation.

which was higher than the collection efficiency without RBCs. This result may seem counterintuitive. When a suspension of RBCs flows in a microchannel, the fluid is strongly mixed by the hydrodynamic interactions between RBCs, as reported in our previous studies.[16,26] Thus, the presence of RBCs likely prevents the inertial migration of cancer cells. On the other hand, cancer cells require a much longer travel distance to show inertial migration as compared with rigid spheres.[26] That is, cancer cells around the center of the channel hardly migrate towards the equilibrium positions. We think that these cells were mixed by the interactions with RBCs and sometimes pushed away from the center. Inertial migration forces acted on these cells, and eventually the cells drifted towards the equilibrium positions. The tendency of increasing collection efficiency with increasing Hct is preferable in achieving high collection efficiency of cancer cells from a RBC suspension.

We should note that the effect of cell–cell interactions cannot be neglected even with a 1% Hct sample, when the microchannel is sufficiently long compared to the width of the channel. This fact can be explained as follows. Let us consider a sphere of diameter d placed in simple shear flow with the shear rate $\dot{\gamma}$. The sphere may interact (or collide) with another sphere, when the center–center distance between the two spheres comes close to about d. The relative velocity of two spheres with the offset of d in the velocity gradient direction is $d\dot{\gamma}$. Thus, the volume V swept out by the sphere in the time period of Δt may be roughly estimated by the product of the cross section, the relative velocity and the time period as $V = \pi d^3\dot{\gamma}\Delta t$. The volume fraction of spheres c and the number density of spheres n can be correlated as $c = \pi d^3 n/6$. By assuming one collision within Δt, nV has to be unity, which leads to $nV = 6c\dot{\gamma}\Delta t = 1$. When $c = 0.01$, *i.e.* 1% Hct, the sphere interacts with another sphere in the time scale of $\Delta t = 1/(0.06\dot{\gamma})$. Let a sphere flow with a velocity U in a channel with half-width W and length L. The travel time T of the sphere flowing through the channel is $T = L/U$. The number of collisions N can be given by $N = T/\Delta t$. By assuming $\dot{\gamma} \approx 2U/W$, N can be estimated as $N = 0.12L/W$. In the present study, the stenosed channel before bifurcation B1 has the dimensions: $W =$ 40 μm and $L = 7.7$mm [*cf.* Fig. 2(a)]. By substituting these values, we can estimate that N is about 23. It means that a sphere experiences near-field collisions about 23 times while flowing through the stenosed channel. We thus think that the effect of cell–cell interactions appears considerably even with a 1% Hct sample in our experimental setup.

Lastly, we compare our results with former studies. In the present study, the collection efficiency of cancer cells with 1% Hct was about 85% [*cf.* eqn (2)]. This value is close to former study done by Bhagat *et al.*,[3] in which MCF-7 cells were separated by utilizing pinched and inertial migration effects. The enrichment of cancer cells was also calculated by comparing the ratio of cancer cells to RBCs in the original sample and that in a sample collected from the cancer-outlet [*cf.* eqn (3)]. The enrichment of cancer cells in this study was about 120 ± 40-fold. From Fig. 4(a) (top-left) and (top-right), we also confirm qualitatively that the ratio of cancer cells to RBCs is significantly increased after flowing through the device. By connecting the present device in series, the enrichment can be improved as 120^M, where M is the number of connections. Other popular size-based and immune-mediated CTC sorting techniques typically achieve 10^4–10^6 fold enrichment,[21–23,27,29,31] which corresponds to 2–3 connections of the present device.

The throughput of the device was 565 μL min^{-1}, which is again a similar value to 400 μL min^{-1} reported by Bhagat *et al.*[3] We think that it is easy to parallelize the present device both two and three dimensionally, given that the device size is small and the channel height is constant throughout the device. By connecting the device in parallel, in series and in lamination layers, we can process a much larger sample volume with much less operation time. These results illustrate that the microfluidic device developed in the present study has the potential to achieve high separation efficiency and significant enrichment of cancer cells.

4. Conclusions

In this study, we developed a multistage microfluidic device to separate cancer cells from an RBC suspension using inertial migration forces. The device was able to effectively remove RBCs up to the 1% Hct condition. It also showed high performance in separating rigid spheres and cancer cells from an RBC suspension with 1% Hct with a throughput of 565 μL min^{-1}. The collection efficiency of cancer cells from an RBC suspension was about 85%, and the enrichment of cancer cells was about 120-fold. Further improvements can be easily achieved by parallelizing the device. These results illustrate that the separation of cancer cells from RBCs is possible using only inertial migration forces, thus paving the way for the development of a novel microfluidic device for future CTC tests.

Acknowledgements

This study was supported by Grants-in-Aid for Scientific Research (S) and the NEXT program of JSPS, and Grants-in-Aid from the Inamori Foundation.

References

1 R. Aoki, M. Yamada and M. Yasuda, In-channel focusing of flowing microparticles utilizing hydrodynamic filtration, *Microfluid. Nanofluid.*, 2009, **6**, 571–576.
2 A. A. S. Bhagat, S. S. Kuntaegowdanahalli and I. Papautsky, Inertial microfluidics for continuous particle filtration and extraction, *Microfluid. Nanofluid.*, 2009, **7**, 217–226.
3 A. A. S. Bhagat, H. W. Hou and L. D. Li, Pinched flow coupled shear-modulated inertial microfluidics for high-throughput rare blood cell separation, *Lab Chip*, 2011, **11**, 1870–1878.
4 G. T. Budd, M. Cristofanilli and M. J. Ellis, Circulating tumor cells *versus* imaging—predicting overall survival in metastatic breast cancer, *Clin. Cancer Res.*, 2006, **12**, 6403–6409.
5 D. D. Carlo, D. Irimia, R. G. Tompkins and M. Toner, Continuous inertial focusing, ordering, and separation of particles in microchannels, *Proc. Natl. Acad. Sci. U. S. A.*, 2007, **104**, 18892–18897.
6 D. D. Carlo, J. F. Edd and D. Irimia, Equilibrium separation and filtration of particles using differential inertial focusing, *Anal. Chem.*, 2008, **80**, 2204–2211.
7 D. D. Carlo, Inertial microfluidics, *Lab Chip*, 2009, **9**, 3038–3046.
8 M. Cristofanilli and G. T. Budd, Circulating Tumor cells, disease progression, and survival in metastatic breast cancer, *N. Engl. J. Med.*, 2004, **351**, 781–791.
9 M. Cristofanilli, D. F. Hayes and G. T. Budd, Circulating Tumor Cells: A novel prognostic factor for newly diagnosed metastatic breast cancer, *J. Clin. Oncol.*, 2005, **23**, 1420–1430.
10 H. Fujiwara, T. Ishikawa and R. Lima, Red blood cell motions in high-hematocrit blood flowing through a stenosed microchannel, *J. Biomech.*, 2009, **42**, 838–843.
11 D. R. Gossett, W. M. Weaver and A. J. Mach, Label-free cell separation and sorting in microfluidic systems, *Anal. Bioanal. Chem.*, 2010, **397**, 3249–3267.
12 S. C. Hur, H. T. K. Tse and D. D. Carlo, Sheathless inertial cell ordering for extreme throughput flow cytometry, *Lab Chip*, 2010, **10**, 274–280.
13 T. Ishikawa and H. Fujiwara, Asymmetry of blood flow and cancer cell adhesion in a microchannel with symmetric bifurcation and confluence, *Biomed. Microdevices*, 2011, **13**, 159–167.
14 S. S. Kuntaegowdanahalli and A. A. S. Bhagat, Inertial microfluidics for continuous particle separation in spiral microchannels, , *Lab Chip*, 2009, **9**, 2973–2980.
15 R. Lima and S. Wada, In vitro blood flow in a rectangular PDMS microchannel: experimental observations using a confocal micro-PIV system, Biomed. , *Biomed. Microdevices*, 2008, **10**, 153–167.
16 R. Lima and T. Ishikawa, Radial dispersion of red blood cells in blood flowing through glass capillaries: The role of hematocrit and geometry, *J. Biomech.*, 2008, **41**, 2188–2196.
17 A. J. Mach and D. D. Carlo, Continuous scalable blood filtration device using inertial microfluidics, , *Biotechnol. Bioeng.*, 2010, **107**, 302–311.
18 J. M. Martel and M. Toner, Inertial focusing dynamics in spiral microchannels, , *Phys. Fluids*, 2012, **24**, 032001.
19 J. P. Matas and J. F. Morris, Inertial migration of rigid spherical particles in Poiseuille flow, , *J. Fluid Mech.*, 2004, **515**, 171–195.
20 J. P. Matas and J. F. Morris, Lateral force on a rigid sphere in large-inertia laminar pipe flow, , *J. Fluid Mech.*, 2009, **621**, 59–67.
21 H. Mohamed, Isolation of tumor cells using size and deformation, , *J. Chromatogr., A*, 2009, **1216**, 8289–8295.
22 S. Nagrath, *et al.*, Isolation of rare circulating tumour cells in cancer patients by microchip technology, , *Nature*, 2007, **450**, 1235–1239.
23 P. Paterlini-Brechot and N. L. Benali, Circulating tumor cells (CTC) detection: Clinical impact and future directions, , *Cancer Lett.*, 2007, **253**, 180–204.
24 E. D. Pratt, C. Huang and B. G. Hawkins, Rare cell capture in microfluidic devices, , *Chem. Eng. Sci.*, 2011, **66**, 1508–1522.
25 G. Segre and A. Silberberg, Behaviour of macroscopic rigid spheres in Poiseuille flow, , *J. Fluid Mech.*, 1962, **14**, 136–157.
26 M. Saadatmand and T. Ishikawa, Fluid particle diffusion through high-hematocrit blood flow within a capillary tube, , *J. Biomech.*, 2011, **44**, 170–175.
27 S. Tan, *et al.*, Microdevice for the isolation and enumeration of cancer cells from blood, , *Biomed. Microdevices*, 2009, **11**, 883–892.
28 T. Tanaka, T. Ishikawa and K. Numayama-Tsuruta, Inertial migration of cancer cells in blood flow in microchannels, , *Biomed. Microdevices*, 2012, **14**, 25–33.
29 G. Vona, Isolation by size of epithelial tumor cells : a new method for the immunomorphological and molecular characterization of circulatingtumor cells, , *Am. J. Pathol.*, 2000, **156**, 57–63.
30 C. Wittekind and M. Neid, Cancer Invasion and Metastasis, , *Oncology*, 2005, **69**, 14–16.
31 S. Zheng, Membrane microfilter device for selective capture, electrolysis and genomic analysis of human circulating tumor cells, , *J. Chromatogr., A*, 2007, **1162**, 154–161.

This journal is © The Royal Society of Chemistry 2012

Digestive Endoscopy (2012) ••, ••–••

doi:10.1111/j.1443-1661.2012.01375.x

ORIGINAL ARTICLE

EXPERIMENTAL APPLICATION OF PULSED LASER-INDUCED WATER JET FOR ENDOSCOPIC SUBMUCOSAL DISSECTION: MECHANICAL INVESTIGATION AND PRELIMINARY EXPERIMENT IN SWINE

CHIAKI SATO,[1] TORU NAKANO,[1] ATSUHIRO NAKAGAWA,[2] MASATO YAMADA,[1] HIROAKI YAMAMOTO,[3] TAKASHI KAMEI,[1] GO MIYATA,[1] AKIRA SATO,[1] FUMIYOSHI FUJISHIMA,[5] MASAAKI NAKAI,[4] MITSUO NIINOMI,[4] KAZUYOSHI TAKAYAMA,[3] TEIJI TOMINAGA[2] AND SUSUMU SATOMI[1]

[1]*Division of Advanced Surgical Science and Technology,* [2]*Department of Neurosurgery, Tohoku University Graduate School of Medicine,* [3]*Interdisciplinary Shock Wave Application Research Division, Institute of Fluid Science,* [4]*Department of Biomaterial Science, Institute for Material Science, Tohoku University and* [5]*Department of Pathology, Tohoku University School of Medicine, Sendai, Japan*

Background and Aim: A current drawback of endoscopic submucosal dissection (ESD) for early-stage gastrointestinal tumors is the lack of instruments that can safely assist with this procedure. We have developed a pulsed jet device that can be incorporated into a gastrointestinal endoscope. Here, we investigated the mechanical profile of the pulsed jet device and demonstrated the usefulness of this instrument in esophageal ESD in swine.

Methods: The device comprises a 5-Fr catheter, a 14-mm long stainless steel tube for generating the pulsed water jet, a nozzle and an optical quartz fiber. The pulsed water jet was generated at pulse rates of 3 Hz by irradiating the physiological saline (4°C) within the stainless steel tube with an holmium-doped yttrium-aluminum-garnet (Ho:YAG) laser at 1.1 J/pulse. Mechanical characteristics were evaluated using a force meter. The device was used only for the part of submucosal dissection in the swine ESD model. Tissues removed using the pulsed jet device and a conventional electrocautery device, and the esophagus, were histologically examined to assess thermal damage.

Results: The peak impact force was observed at a stand-off distance of 40 mm (1.1 J/pulse). ESD using the pulsed jet device was successful, as the tissue specimens showed precise dissection of the submucosal layer. The extent of thermal injury was significantly lower in the dissected bed using the pulsed jet device.

Conclusion: The results showed that the present endoscopic pulsed jet system is a useful alternative for a safe ESD with minimum tissue injury.

Keywords: early esophageal tumor, endoscopic submucosal dissection (ESD), holmium-YAG laser, medical engineering, minimally invasive surgery, therapeutic endoscopy.

INTRODUCTION

Endoscopic submucosal dissection (ESD)[1] is an emerging, minimally invasive therapeutic technique for en bloc resection of gastrointestinal tract lesions, including early-stage esophageal cancer. In spite of the advantages of ESD over conventional techniques, such as endoscopic mucosal resection (EMR), it requires highly advanced techniques and a learning curve exists for the performance of ESD; it has been estimated that endoscopists need to operate on 30 patients under the supervision of an expert to overcome this learning curve.[2,3] In addition, lack of instruments that can assist in this procedure without the risk of potential complications (thermal injury and vascular damage) is one of the drawbacks of the current ESD technique.[4] Therefore, new equipment that will facilitate the accomplishment of ESD without requiring special training and minimizing the risk of complications is highly desirable.

Water jet technology, based on conventional pressure-driven continuous jet[5,6] or laser/electrically induced pulsed pressure,[7–9] provides an alternative method for dissecting soft tissues without damaging small vessels or causing mechanical and thermal damage. Moreover, precise tissue dissection together with preservation of vessels and nerves can be achieved.[10,11] Conventional pressure-driven continuous water jet technology has already been applied for endoscopic treatment.[12] However, its use was limited to transmucosal injection of water into the submucosal layer to elevate the mucosa in preparation for EMR rather than for tissue dissection,[13,14] probably due to the continuous nature of the water jet. The use of continuous water flow also carries the potential risk of obscuring the narrow endoscopic operative view.

Pulsed laser-induced water jet is a novel alternative to achieve tissue dissection with a significantly lower amount of water.[15] We have already achieved significant reduction of intraoperative blood loss and procedure time in the field of neurosurgery, despite a significant increase in the tumor removal rate.[9] The pulsed laser-induced water jet device enables tissue dissection without thermal damage while preserving small vessels.[15,16] Therefore, we have developed the endoscopic pulsed jet system for ESD. The purposes of the present study are to develop a device that can be incorporated into a gastrointestinal endoscope, to clarify the mechanical profile of the pulsed jet from this device, and to demonstrate its usefulness in ESD carried out in a swine model.

Correspondence: Toru Nakano, Division of Advanced Surgical Science and Technology, Tohoku University Graduate School of Medicine, 1-1, Seiryo-machi, Aoba-ku, Sendai, Miyagi 980-8574, Japan. Email: torun@med.tohoku.ac.jp

Received 30 December 2011; accepted 1 August 2012.

METHODS

Pulsed jet device for gastrointestinal endoscopes

Figure 1A is a schematic diagram of the pulsed laser-induced jet system. Figure 1B is a photograph of the pulsed jet device and tip of the nozzle. The device consists of a 5-Fr catheter (RH-5AP4561; Terumo Corporation, Tokyo, Japan) incorporating a jet generator made of a stainless steel tube (19-G stainless steel tube, 0.9 mm internal ø, 1.26 mm external ø, length 14 mm, SUS304; Techno Science, Sendai, Japan) and an optical quartz fiber (400 μm core ø, NO.QL-400-850-5; Sparkling Photon, Tokyo, Japan), leading into a polytetrafluoroethylene (PTFE) tapered nozzle (exit 0.5 mm internal ø, inlet 1 mm internal ø). Two PTFE tubes (7–306-01 and 7–306-02; AZ One Corp., Osaka, Japan) (Fig. 1B left, bottom) were combined. This device was assembled from the distal end in the following order: the PTFE tubes, stainless steel tube, and 5-Fr catheter. The inner capillary structure was placed in the proximal end of the metal tube to prevent reverse water jet flow and thereby improve the impact force of the pulsed jet (Fig. 1A). The internal diameter of the tube was tapered from 1 mm at the entry to 0.5 mm at the exit. Because this system is intended to be incorporated into a gastrointestinal endoscope, the length of the metal tube was 14 mm to preserve the flexibility of the gastrointestinal endoscope. The proximal end of the catheter was sealed with a Y connector (AP-YC25S; Terumo Corporation) to prevent air from entering the system. Cold physiological saline (4°C) was supplied at 100 mL/h through an inner capillary by a syringe pump (TE-331S; Terumo Corporation) (Fig. 1B). Physiological saline was kept at 4°C to prevent thermal damage.[16]

The jet energy source was a pulsed holmium-doped yttrium-aluminum-garnet (Ho:YAG) laser system (model SLS-HO; Sparkling Photon, Tokyo, Japan) with a wavelength of 2.1 μm, pulse duration of 350 μs.

Measurement of mechanical profiles

The dynamics of the jet was initially confirmed using a high-speed camera (HPV-1; Shimadzu Corporation, Kyoto, Japan). The mechanical profile of the pulsed liquid jet generated by the endoscopic pulsed jet system was evaluated using a force meter (PFDT-200GF; Sparkling Photon). The nozzle of the endoscopic pulsed jet device was placed perpendicular to the force meter using a holder and the tip of the nozzle was placed 10 mm away. The impact force of the jet was calculated with software that analyzed the time sequence observation of the impact of a single shot detected by the force meter and demonstrated on the oscilloscope (TDS3014B; Tektronix, Tokyo, Japan). The relationship between the stand-off distance (the distance between the tip of the nozzle and the optical fiber), laser energy and impact force of the liquid jet was evaluated. The stand-off distance was changed from 20 to 150 mm by 20 mm increments according to previous experiments.[8]

Esophageal ESD in swine

Three domestic pigs (*Sus scrofa domesticus* LWD, 12–14 weeks old, 30–40 kg) were used in this study. All animal procedures and protocols were approved by the institutional review board of the Center for Laboratory Animal Research of Tohoku University.

The endoscopic pulsed jet was applied at a frequency of 3 Hz and at a laser energy of 1.1 J/pulse. The stand-off

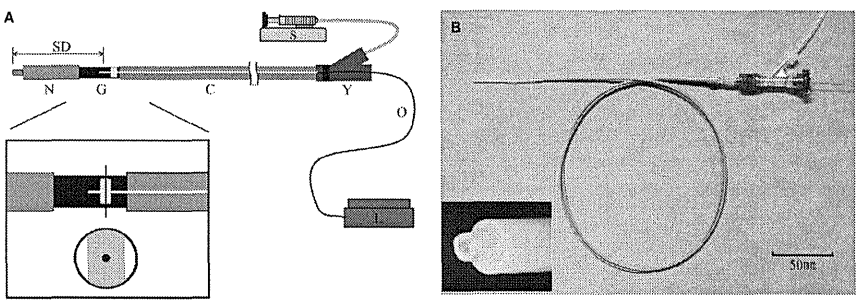

Fig. 1. (A) Schematic diagram of the laser-induced pulsed jet system. N, nozzle (exit; 0.5 mm inner ø, 1.0 mm outer ø, inlet; 1.0 mm inner ø, 2.0 mm outer ø); G, pulsed jet generator made of stainless steel tube; C, Flexible catheter (0.9 mm inner ø); O, optical quartz fiber (0.4 mm core ø); Y, Y-connector; S, syringe pump; SD, stand-off distance; L, pulsed holmium-doped yttrium-aluminum-garnet (Ho:YAG) laser system. Inset: lateral sectional view (upper) and cross-sectional view (lower) of the pulsed jet generator. (B) Photograph of the laser-induced pulsed water jet device. Inset: Photograph of the nozzle. Two polytetrafluoroethylene tubes were combined. Tip of nozzle was tapered (exit: 0.5 mm inner ø, inlet: 1.0 mm outer ø).

distance was fixed at 100 mm. Cold physiological saline (4°C) was supplied at a rate of 100 mL/h using a syringe pump. Parameter settings were derived in preliminary experiments in which various stand-off distances and laser energy were examined at the time of dissection of resected swine esophagus (data not shown).

The pulsed jet device was incorporated into a gastrointestinal endoscope (GIF-Q260; Olympus Medical Systems, Tokyo, Japan) and esophageal ESD was carried out in healthy domestic pigs under general anesthesia with controlled ventilation. They were anesthetized with 0.04 mg/kg medetomidine chloride, 0.4 mg/kg midazolam and 0.2 mg buprenorphine hydrochloride. Isoflurane gas was used for maintenance of anesthesia during the procedure (model PH-3F; Acoma Co., Tokyo, Japan) under mechanical ventilation (ARF-900; Acoma Co.). Vital signs including blood pressure and oxygen saturation were monitored. Tissue specimens were extirpated by conventional methods [electrocautery device (KD-620LR; Olympus Medical Science Corporation, Tokyo, Japan)] (control group) and by the pulsed jet device (pulsed jet group). First, each target area (simulated lesion) was similarly marked with electrocautery in both groups. In the pulsed jet group, targets were marked at 40 cm from the dental arch, and in the control group, targets were marked at 30 cm. Then, after submucosal injection of physiological saline combined with 0.4% indigocarmine to separate the target tissue from the muscularis propria, initial cuts (so-called pre-cuts) were carried out into the submucosal layer with an electrocautery system (SurgiStat™ II; Covidien Co., Mansfield, MA, USA) in cutting mode at 100 W. In both groups, a circumferential incision into the submucosa around the lesion was made outside the initial marking using the electrocautery device in coagulation mode at 60 W. The submucosal dissection was carried out with an electrocautery device in the control group, and with the pulsed jet device in the pulsed jet group. Otherwise, procedures were all the same in both groups. In the present study, the pulsed jet device was used only for dissecting the submucosa. The operative endoscopic view of submucosal dissection with the endoscopic pulsed jet device is shown in Figure 2. The pulsed jet device has no hemostatic ability; to control bleeding, a hemostatic device (FD-410LR; Olympus Medical Science Corporation) was used in coagulation mode at 60 W in both procedures. The swine were killed after ESD by both methods; each resection bed was cut into pieces 3 mm wide and the fixed specimens were embedded in paraffin blocks, then cut parallel to the longitudinal side into sections 3 μm thick. Each section was stained with hematoxylin-eosin and elastica-Masson stain before examination by optical microscopy to evaluate the morphological characteristics of the dissection (general dissection structure and quality of the dissection margins). Degeneration of muscle fibers (alteration of architecture, non-homogeneous coloration, disruption of muscle fibers) indicated thermal injury.[17] The length of degeneration of muscle fibers due to thermal injury was measured in each section.

Presence of thermal damage was compared by χ^2-test. The extent of thermal damage and dissection was measured in each specimen. The extent of thermal damage in the muscular layer and the length of the dissected mucosal layer in each specimen were calculated and compared by Mann–Whitney *U*-test. The level of statistical significance was set at $P < 0.05$.

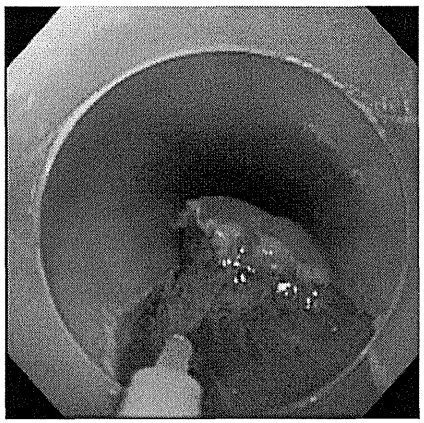

Fig. 2. Operative endoscopic view of submucosal dissection with endoscopic pulsed jet device.

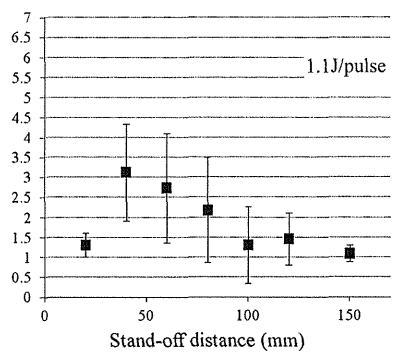

Fig. 3. Relationship between stand-off distance and maximum jet impact force at a laser energy of 1.1 J/pulse. The peak of impact force at a laser energy of 1.1 J/pulse was observed at a stand-off distance of 40 mm.

All calculations were carried out using StatView J-5.0 (SAS Institute, Cary, NC, USA).

RESULTS

Measurement of mechanical profiles

Figure 3 shows the relationship between stand-off distance and impact force of the jet at 1.1 J/pulse. In the present experiment, the peak impact force was 3.13 ± 1.22 N at the stand-off distance of 40 mm. However, an appropriate setting for dissection of swine esophagus was 1.3 ± 0.9 N at the stand-off distance of 100 mm. This setting was derived from preliminary experiments in which various stand-off distances and laser energy were examined at the time of dissection of resected swine esophagus (data not shown). The impact force of the jet increased in proportion to the increase of the laser energy (data not shown). Capillary structure increased the impact force of the jet approximately by 200% (data not shown).

Esophageal ESD in swine

Endoscopic submucosal dissection using the pulsed jet device was successful. The impact force of the pulsed jet was strong enough to dissect the submucosal layer (1.1 J/pulse and stand-off distance 100 mm, impact force 1.3 ± 0.9 N), while preserving small vessels and causing no harmful bleeding. Electrocautery device was only used to coagulate these isolated small vessels in the pulsed jet group. The endoscopic view of the surgical field was acceptable, as it was kept clean and showed that the pulsed jet device could dissect the submucosa while in contact with it or 2 to 3 mm apart from it.

A total of six ESD procedures were carried out (three by electrocautery device, three by pulsed jet device). The mean diameter of the resected mucosa did not differ significantly between the pulsed jet group and the control group (20.0 ± 8.7 mm, 21.0 ± 12.1 mm, $P = 0.9$). In both groups, specimens were dissected just on the surface of the muscle layer as shown in Figure 4. Macroscopic thermal damage in the pulsed jet group was less than that in the control group in the submucosal side of the resected specimens (Fig. 5). The en bloc resection rate was 100% in both groups. The duration of the procedure in the pulsed jet group was 50.7 ± 29.9 min, and in the control group it was 31.3 ± 16.4 min ($P = 0.38$). There was no uncontrollable bleeding or perforation in any ESD procedure. Thermal damage of the resection bed differed depending on the tissue surface (Fig. 4). Figure 4a–d shows degeneration of the inner muscularis propria (alteration of architecture of muscle fibers, non-homogeneous coloration). ESD using the pulsed jet device resulted in almost no thermal damage to the fascia of the muscularis propria (Fig. 4e–h). Twenty-two specimens were examined in each group. The incidence of thermal damage was significantly small in 9.1% of the specimens (2/22) resected by pulsed jet compared to 59.1% (13/22) in the control group ($P = 0.004$). The extent of thermal damage of the muscle layer in relation to that of the dissected submucosal layer was significantly smaller in the pulsed jet group (1.01 ± 4.29%), compared to the control group (15.09 ± 20.60%) ($P = 0.0009$) (Fig. 6).

DISCUSSION

We have successfully shown that a pulsed jet device can be incorporated into a gastrointestinal endoscope. Mechanical investigation revealed that the impact force generated by the device depended on the stand-off distance. We also showed that the pulsed jet device was safely only used for the part of submucosal dissection in the swine ESD model. There was no obvious disturbance of the surgical field by splashing, misting, or aerosol.

Water jet instrumentation, both by pressure-driven continuous jet and the present pulsed method, delivers energy as kinetic energy of the water flow, which is ejected through a small nozzle at the tip of the delivery device. The jet transmits the kinetic energy to the tissue surface and ejects particles of tissue, creating a corridor through the organ; thus, the jet can also be used for mass reduction.[5,18] The water jet instrument possesses several qualities concerning dissection that are superior to those of conventional instruments, such as selective tissue removal with vessel preservation, based on the different tensile strengths of tissues. Pressure-driven continuous water jet technology was initially used in the liver in the 1980s[5] and thereafter it has been used in neurosurgery,[19] stomach,[13] colon,[14] cardiovascular,[20] and ophthalmological[21] surgery. The use of this system in liver surgery results in reduced blood loss and less parenchymal trauma than ultrasonic aspiration or blunt dissection.[22,23] The high quality of dissections carried out with water jet and its efficacy in microsurgical procedures have been demonstrated in the field of neurosurgery.[24] Another notable advantage is the avoidance of thermal damage to the surrounding parenchyma, which is inevitable with electrocautery, electromagnetic field, ultrasonic, and laser instruments.[25,26] Despite these advantages, the size of the pressure-driven continuous water jet device and the amount of water required have prevented its incorporation into minimally invasive instruments (endoscope and catheters).

Our endoscopic pulsed jet system differs from the pressure-driven continuous water jet in its application for removal of a target lesion while preserving small vessels and using a significantly small amount of water; it allows access to deep, narrow operative fields, under either an operating microscope or a neuroendoscope.[15] The Ho:YAG laser is a solid-state laser with a mid-infrared wavelength (2.1 μm) that is close to one of the light-absorption peaks of water at 1.9 μm.[27] Therefore, the laser pulse forms a transient vapor bubble in the water flow, and the three-dimensional expansion of the confined vapor bubble is used to drive a one-dimensional liquid jet through a fine nozzle, thus generating a high-velocity pulsed jet of microliter order.[8,15] We have already reported that tissue penetration depth depends on initial velocity and pressure, which can be controlled by the laser energy, stand-off distance, and nozzle (aspect) ratio.[28,29] In the present experiment, we found that when using the endoscopic pulsed jet device, tissue penetration also depended on those same factors, despite differences in structure.

It was reported that the performance of the pulsed jet was far superior to that of a continuous jet operating under the same parameters.[30] Seto *et al.* also reported that the degree of dissection of the pulse jet was less sensitive to exposure time, which means the pulsed jet is safe and reliable when applied for clinical treatment.[31] These findings might explain why the pulsed water jet can efficiently dissect the submucosa with less water and energy compared to the continuous water jet.

In the pulsed laser-induced water jet, the photothermal energy of the laser is transformed into kinetic energy, thus no photothermal effect occurs, and the temperature of the water jet remains below 41°C,[16] which is the reported temperature during use of the ultrasound aspirator, and is also lower than 43°C, the reported functional threshold of neuronal damage.[32] Bleeding, perforation and postoperative stricture are

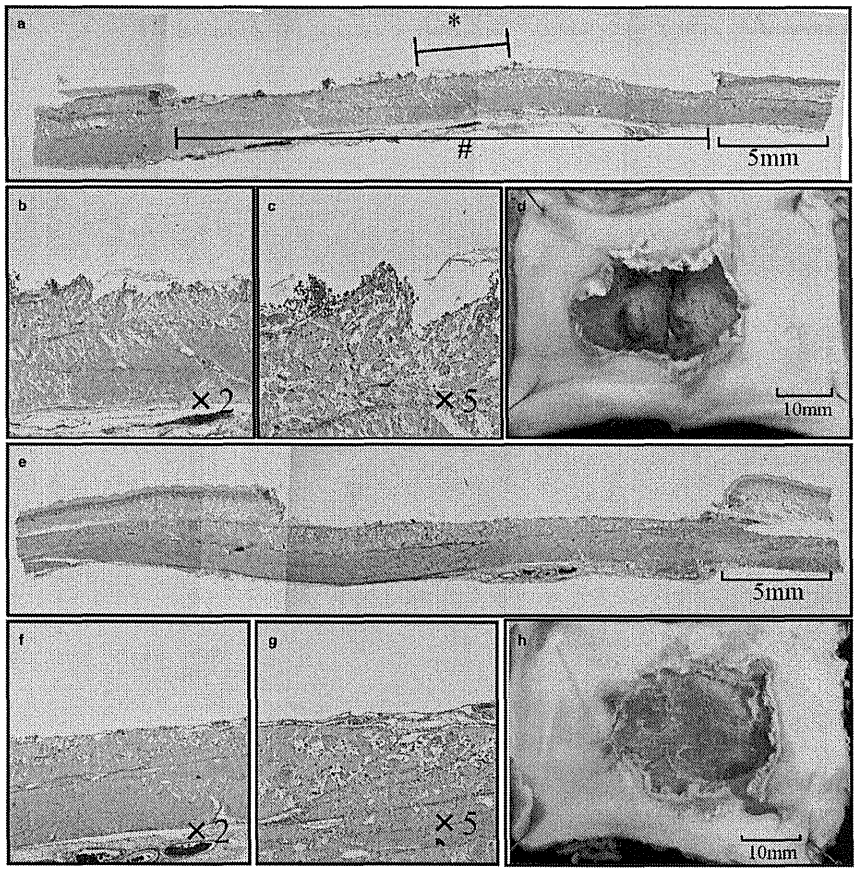

Fig. 4. Microscopic (a, b, c) and macroscopic imaging (d) showing thermal damage in a specimen treated by conventional electrocautery (control group). Thermal damage was recognized at the inner circular muscle layer of the esophagus. *, Extent of thermal damage of the inner circular muscle layer. #, Extent of submucosal dissection. Elastica-Masson staining. Scale bar a: 5 mm, b: original magnification × 2, c: × 5). Microscopic (e, f, g) and macroscopic imaging (h) showing no obvious thermal damage in the specimen treated using the pulsed jet device (pulsed jet group). No obvious thermal damage was recognized in the muscle layer. Elastica-Masson staining. Scale bar e: 5 mm, f: original magnification × 2, g: × 5).

considered the major complications after ESD.[33] The perforation risk is even higher in the stomach,[1] esophagus[33] and colon.[34] Severe inflammation can occur after thermal damage resulting from the use of an electrocautery device. The progression of atrophy and fibrosis in the muscularis propria after inflammation could be a direct effect of damage not only of myofibers, but also of the myenteric nerve plexus.[35] The most effective and simple way to prevent perforation would be to dissect the submucosa without an electrocautery device.[36] In case of electrocoagulation hemostasis during both ESD procedures, surrounding tissues suffered not even minimal thermal damage. In previous studies, we found that a

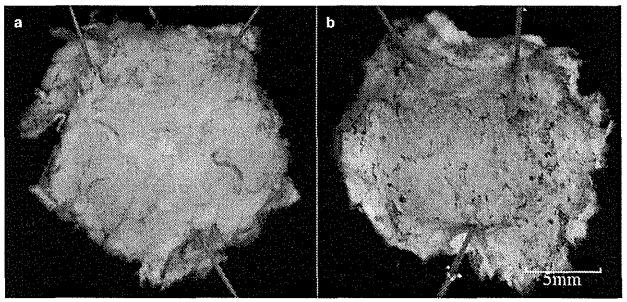

Fig. 5. Photograph of resected specimens (submucosal layer side). (a) Pulsed jet group; (b) control group. Macroscopically, the submucosa of the resected specimen with the pulsed jet device has less thermal damage than that of the control group (a), whereas the submucosa of the resected specimen with the electrocautery device has thermal damage (b).

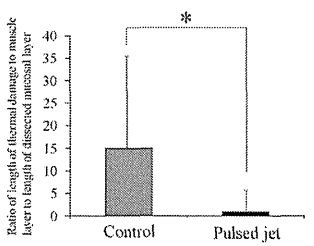

Fig. 6. Extent of thermal damage of the muscle layer in relation to that of the dissected submucosal layer in both groups. The ratio of damage was 1.01% (pulsed jet group) and 15.09% (control group). *P=0.0009.

pulsed laser-induced water jet enabled the surgeon to dissect and debulk a brain tumor while preserving the small vessels down to 100 to 200 μm, which is the minimum diameter of blood vessels preserved using continuous water jet instrumentation.[15,37] Compared to conventional ESD procedures, ESD using the endoscopic pulsed jet system enables exposure of small vessels and coagulation with the electrocautery device; therefore, the number of times the electrocoagulation device is required is potentially decreased, thereby reducing thermal injury of surrounding tissues. While the pulsed jet was injected to the submucosa between 0 and 90 degrees, the muscle layer was not injured at the settings used in this study. The appropriate angle to dissect the submucosa with the pulsed jet device must be investigated in future studies. The present experiment showed that the endoscopic pulsed jet device may become an alternative to removing a target lesion, as thermal damage and the risk of perforation is significantly smaller. Consequently, the endoscopic pulsed jet system offers a new strategy for ESD.

The simplicity of the system is advantageous compared to other competing instruments. Custom-made and personal modification of the applicator with minimal costs broadens the potential future applications of this technology.[9] In the present experiments, the operative view was broader in the pulsed jet device. This was partly attributed not only to the small size of the device, but also to the use of a semi-transparent nozzle. A direct punch with the tip of the device is one of the causes of perforation. The tip of the nozzle is more flexible than the electrocautery device, reducing the risk of perforation due to direct injury.

In the present experiment, we selected the esophagus as the first organ for using the pulsed jet device, because complications of esophageal ESD could become much more serious compared to ESD of other organs in the gastrointestinal tract, such as stomach or colon. We investigated the usefulness and safety of the device in a swine esophageal ESD model. Pulsed jet device can be used in other organs (kidney, liver, stomach and colon), provided the appropriate settings for other organs are clarified in future studies.

Lack of examination of the pathological tissues (i.e. malignancy and fibrosis) and lack of long-term evaluation as well as the small number of animals used are limitations of the present study. Before this device is used in humans, additional short- and long-term animal experiments, including pathological examination, should be carried out.

ACKNOWLEDGMENTS

This work was supported in part by Grants-in-Aid for Scientific Research (B) (No. 18390388) and (No. 19390372), a Grant-in-Aid for Young Scientists (A) (No. 19689028), (22689039), and Challenging Exploratory Research (No. 21659313), (21659334) from the Japanese Ministry of Health, Labour and Welfare, the Japanese Foundation for Research and Promotion of Endoscopy Grant (A), the Tohoku University Exploratory Research Program for Young Scientists (ERYs), the Collaborative Research Project of the Institute of Fluid Science, Tohoku University, Ogino Award of Research Facilitating from Japanese Society of Biomedical Engineering, and SEI Group CSR Foundation.

The authors would like to thank Dr Daisuke Kudo and Kiyonobu Ohtani for valuable comments, and Teruko Sueta, Nobuko Hashimoto, and Yayoi Okano for conducting the experiments.

CONFLICT OF INTERESTS

Authors declare no conflict of interests for this article.

REFERENCES

1. Gotoda T. A large endoscopic resection by endoscopic submucosal dissection procedure for early gastric cancer. *Clin. Gastroenterol. Hepatol.* 2005; **3**: S71–3.
2. Gotoda T, Friedland S, Hamanaka H, Soetikno R. A learning curve for advanced endoscopic resection. *Gastrointest. Endosc.* 2005; **62**: 866–7.
3. Choi IJ, Kim CG, Chang HJ, Kim SG, Kook MC, Bae JM. The learning curve for EMR with circumferential mucosal incision in treating intramucosal gastric neoplasm. *Gastrointest. Endosc.* 2005; **62**: 860–5.
4. Oda I, Gotoda T, Hamanaka H *et al.* Endoscopic submucosal dissection for early gastric cancer: Technical feasibility, operation time and complication from a large consecutive series. *Dig. Endosc.* 2005; **17**: 54–8.
5. Papachristou DN, Barters R. Resection of the liver with a water jet. *Br. J. Surg.* 1982; **69**: 93–4.
6. Oertel J, Gaab MR, Warzok R, Piek J. Waterjet dissection in the brain: Review of the experimental and clinical data with special reference to meningioma surgery. *Neurosurg. Rev.* 2003; **26**: 168–74.
7. Miller JM, Palanker DV, Vankov A, Marmor MF, Blumenkranz MS. Precision and safety of the pulsed electron avalanche knife in vitreoretinal surgery. *Arch. Ophthalmol.* 2003; **121**: 871–7.
8. Hirano T, Komatsu M, Saeki T *et al.* Enhancement of fibrinolytics with a laser-induced liquid jet. *Lasers Surg. Med.* 2001; **29**: 360–8.
9. Ogawa Y, Nakagawa A, Takayama K, Tominaga T. Pulsed laser-induced liquid jet for skull base tumor removal with vascular preservation through the transsphenoidal approach: A clinical investigation. *Acta Neurochir. (Wien)* 2011; **153**: 823–30.
10. Piek J, Oertel J, Gaab MR. Waterjet dissection in neurosurgical procedures: Clinical results in 35 patients. *J. Neurosurg.* 2002; **96**: 690–6.
11. Tschan C, Gaab MR, Krauss JK, Oertel J. Waterjet dissection of the vestibulocochlear nerve: An experimental study. *J. Neurosurg.* 2009; **110**: 656–61.
12. Neuhaus H, Wirths K, Schenk M, Enderle MD, Schumacher B. Randomized controlled study of EMR versus endoscopic submucosal dissection with a water-jet hybrid-knife of esophageal lesions in a porcine model. *Gastrointest. Endosc.* 2009; **70**: 112–20.
13. Kaehler GF, Sold MG, Fischer K, Post S, Enderle M. Selective fluid cushion in the submucosal layer by water jet: Advantage for endoscopic mucosal resection. *Eur. Surg. Res.* 2007; **39**: 93–7.
14. Yahagi N, Neuhaus H, Schumacher B *et al.* Comparison of standard endoscopic submucosal dissection (ESD) versus an optimized ESD technique for the colon: An animal study. *Endoscopy* 2009; **41**: 340–5.
15. Ohki T, Nakagawa A, Hirano T *et al.* Experimental application of pulsed Ho : YAG laser-induced liquid jet as a novel rigid neuroendoscopic dissection device. *Lasers Surg. Med.* 2004; **34**: 227–34.
16. Hirano T, Nakagawa A, Uenohara H *et al.* Pulsed liquid jet dissector using holmium:YAG laser–a novel neurosurgical device for brain incision without impairing vessels. *Acta Neurochir. (Wien)* 2003; **145**: 401–6. discussion 406.
17. Lequerica JL, Sanz E, Hornero F *et al.* Esophagus histological analysis after hyperthermia-induced injury: Implications for cardiac ablation. *Int. J. Hyperthermia* 2009; **25**: 150–9.
18. Oertel J, Gaab MR, Knapp A, Essig H, Warzok R, Piek J. Water jet dissection in neurosurgery: Experimental results in the porcine cadaveric brain. *Neurosurgery* 2003; **52**: 153–9. discussion 159.
19. Terzis AJ, Nowak G, Rentzsch O, Arnold H, Diebold J, Baretton G. A new system for cutting brain tissue preserving vessels: Water jet cutting. *Br. J. Neurosurg.* 1989; **3**: 361–6.
20. Aroussi AA, Sami IM, Leguerrier A, Verhoye JP. The blower: A useful tool to complete thrombectomy of the mechanical prosthetic valve. *Ann. Thorac. Surg.* 2006; **81**: 1911–2.
21. Lipshitz I, Bass R, Loewenstein A. Cutting the cornea with a waterjet keratome. *J. Refract. Surg.* 1996; **12**: 184–6.
22. Izumi R, Yabushita K, Shimizu K *et al.* Hepatic resection using a water jet dissector. *Surg. Today* 1993; **23**: 31–5.
23. Rau HG, Duessel AP, Wurzbacher S. The use of water-jet dissection in open and laparoscopic liver resection. *HPB (Oxford)* 2008; **10**: 275–80.
24. Oertel J, Gen M, Krauss JK, Zumkeller M, Gaab MR. The use of waterjet dissection in endoscopic neurosurgery. Technical note. *J. Neurosurg.* 2006; **105**: 928–31.
25. Oertel J, Gaab MR, Pillich DT, Schroeder HW, Warzok R, Piek J. Comparison of waterjet dissection and ultrasonic aspiration: An in vivo study in the rabbit brain. *J. Neurosurg.* 2004; **100**: 498–504.
26. Schurr MO, Wehrmann M, Kunert W *et al.* Histologic effects of different technologies for dissection in endoscopic surgery: Nd:YAG laser, high frequency and water-jet. *Endosc. Surg. Allied Technol.* 1994; **2**: 195–201.
27. Jansen ED, van Leeuwen TG, Motamedi M, Borst C, Welch AJ. Temperature dependence of the absorption coefficient of water for midinfrared laser radiation. *Lasers Surg. Med.* 1994; **14**: 258–68.
28. Nakagawa A, Hirano T, Komatsu M *et al.* Holmium: YAG laser-induced liquid jet knife: Possible novel method for dissection. *Lasers Surg. Med.* 2002; **31**: 129–35.
29. Nakagawa A, Kumabe T, Kanamori M *et al.* Clinical application of pulsed laser-induced liquid jet: Preliminary report in glioma surgery. *Neurol. Surg.* 2008; **36**: 1005–10. [Article in Japanese].
30. Foldyna J, Sitek L, Svehla B, Svehla S. Utilization of ultrasound to enhance high-speed water jet effects. *Ultrason. Sonochem.* 2004; **11**: 131–7.
31. Seto T, Yamamoto H, Takayama K, Nakagawa A, Tominaga T. Characteristics of an actuator-driven pulsed water jet generator to dissecting soft tissue. *Rev. Sci. Instrum.* 2011; **82**: 055105.
32. Matsumi N, Matsumoto K, Mishima N *et al.* Thermal damage threshold of brain tissue–histological study of heated normal monkey brains. *Neurol. Med. Chir. (Tokyo)* 1994; **34**: 209–15.
33. Fujishiro M, Yahagi N, Kakushima N *et al.* Endoscopic submucosal dissection of esophageal squamous cell neoplasms. *Clin. Gastroenterol. Hepatol.* 2006; **4**: 688–94.
34. Taku K, Sano Y, Fu KI *et al.* Iatrogenic perforation associated with therapeutic colonoscopy: A multicenter study in Japan. *J. Gastroenterol. Hepatol.* 2007; **22**: 1409–14.
35. Honda M, Nakamura T, Hori Y *et al.* Process of healing of mucosal defects in the esophagus after endoscopic mucosal resection: Histological evaluation in a dog model. *Endoscopy* 2010; **42**: 1092–5.
36. Yamasaki M, Kume K, Yoshikawa I, Otsuki M. A novel method of endoscopic submucosal dissection with blunt abrasion by submucosal injection of sodium carboxymethylcellulose: An animal preliminary study. *Gastrointest. Endosc.* 2006; **64**: 958–65.
37. Nakagawa A, Hirano T, Jokura H *et al.* Pulsed holmium:yttrium-aluminum-garnet laser-induced liquid jet as a novel dissection device in neuroendoscopic surgery. *J. Neurosurg.* 2004; **101**: 145–50.

周術期放射線治療や周術期の栄養管理 *

keywords：術前放射線化学療法、ERAS、術前絶飲食

中野 徹[1)] Toru NAKANO　　宮田 剛[2)] Go MIYATA

◆東北大学病院　移植・再建・内視鏡外科[1)]　東北大学大学院先進外科学分野[2)]
Department of Organ Transplantation, Reconstruction and Endoscopic Surgery, Tohoku University Hospital[1)]
Division of Advanced Surgical Science and Technology, Tohoku University, Graduate school of Medicine[2)]

種々の癌において周術期に施行される放射線療法や化学療法の有効性が報告されており、原疾患に起因する栄養障害とこれら補助療法による有害事象を考慮し栄養管理を行う必要が生じている。従来の周術期管理の基本的な考え方は主に術後の栄養管理によって手術侵襲に伴う異化亢進による蛋白喪失を軽減し術後の回復を促進することが目的であったが、最近では術前、術中から栄養管理を積極的に行うことで侵襲の低下のみならず長期予後にも影響を及ぼすことが明らかにされている。欧州での大腸がんを対象とした術後早期回復プロトコル(ERAS)においても栄養管理は重要な位置を占めており、栄養投与のみならず腸管機能促進と侵襲軽減や感染症の低下が報告されている。さらに術前の絶食期間を短縮することにより術後早期からの腸管機能回復に役立つという報告がなされてきている。これらを周術期合併療法とうまく組み合わせていくことが必要となる。

はじめに

癌の治療において集学的治療の一環として、あるいは周術期に行われる補助療法として放射線療法が単独あるいは化学療法と併用され行われることがある。周術期に行われる補助療法の目的は腫瘍を縮小させて主治療である手術の効果を向上させることにあるが、生存率の向上、再発率の低下、臓器温存率の向上、あるいはQOLの向上など、目的は標的とするがんの種類によって多少異なる。近年、腫瘍に線量を集中し、周囲の正常組織への線量を低下させるなどの工夫により有害事象を減らすことも可能となってきている[1)]。従来は放射線照射が行われなかった癌に対して広く行われたり、化学療法との組み合わせにより術前術後照射が行われたりするようになってきている。一方で化学療法と照射療法を併用した場合は副作用や術後合併症の頻度は高くなることが報告されており[2) 3)]効果を期待するとともに有害事象に注意が必要である。術前からの栄養評価と栄養療法の介入が周術期に必要とされている。

周術期の放射線療法

1.頭頸部癌における放射線療法

頭頸部に含まれる癌は、舌癌、喉頭癌、下咽頭癌、甲状腺癌などがあり、そのほかに、中咽頭癌、上咽頭癌、上顎癌などがこれに次ぐ。喉頭癌は早期では放射線治療あるいは部分切除が、進行癌では喉頭全摘あるいは放射線と手術を組み合わせた集学的治療が行われている[4)]。臓器機能温存率の向上を目指した放射線化学療法がおこなわれる一方で放射線化学療法の効果を判定し手術が必要な症例には救済手術も試みられている[5)]。

*Perioperative radiation therapy and nutritional management

2.食道癌に対する放射線療法

従来食道癌に対する術前照射は手術による根治切除率を上げる目的で原発巣の気管浸潤や大血管への浸潤が疑われる症例に行われていたが、手術可能な症例にも行われるようになってきた。補助療法としての術前照射単独の効果については本邦のRCTにおいて効果はみとめられていないが[6)]、欧米では抗癌剤との併用で効果が報告されている[7)~9)]。通常欧米や我が国ではCDDPと5FUを組み合わせたプロトコールが広く行われているが最近カルボプラチンとパクリタキセルとの併用で良好な成績も報告されている[10)]。線量は30−50gyとする報告が多いが投与量やスケジュールは一定していない。照射野に関しては局所照射野(気腫型)、T字照射野などがある。病変の局在やリンパ節転移状況、全身状態によっても変わり施設間でも異なる。根治的放射線化学療法を施行したのちの局所再燃に対する手術療法として救済食道切除術(salvage esophagectomy)が近年施行されるようになった。治癒切除が行われれば予後が期待でき早期に救済可能な再発を発見することの重要性が高くなっているが[11)]、放射線照射による影響の為、縫合不全と呼吸器合併症が多く、在院死亡率も手術単独に比して多い[12) 13)]。根治的放射線化学療法を施行する際は後に手術の可能性があることも念頭に置いて全身状態と栄養状態の管理が必要である。

3.直腸癌に対する放射線化学療法

進行直腸癌に対して術前に放射線化学療法(50-60 gy)を行うことで、生存率や肛門温存率を向上させることが報告されており[14)~16)]、術後のQOLに大きな貢献をする可能性がある。直腸に対する放射線化学療法は術前と術後では生存率に変わりはないが[17)]、術前に行うほうが有害事象が少ないため[18)]適応症例には術前に施行すべきであるようだ。

放射線照射による有害事象

放射線による有害事象は一般的に照射部位や範囲により種類や発症順が左右され、照射線量に応じて重症度が異なる[19)]。放射線化学療法の有害事象は大きく分けて早期と晩期に分けられる。早期の有害事象は放射線食道炎や骨髄抑制、消化器毒性などがある。晩期有害事象は胸膜炎や心嚢液貯留、放射線脊髄炎などがあり治療後数か月から数年で徐々に発症するが、数十年を経て発症することもある。周術期に問題となる有害事象は早期に生じる有害事象であるが、術後の経過観察をする上で、晩期障害にも注意を払わなければいけない。

1.放射線食道炎

通常照射開始後数週間より出現し、照射終了後1か月程度で改善するといわれている。化学療法を併用している場合は発症頻度はより高くなる傾向にあり(1)発症率は19-27%と最近報告されている。発症時の線量については20 gy以下で19.6%、20-30 gyで37%、30-40 gyで13%、40-50 gyで15%と報告されており[20)]、根治照射に比べて低線量を用いる周術期の照射によっても食道炎は高率に発症している。症状は安静時疼痛、嚥下時痛、粘膜浮腫、それに伴う狭窄による経口摂取低下、経口摂取不能といった状態になり栄養状態の低下を生じることになり治療期間中の生活の質を著しく低下させる[21)]。疼痛は非常に強くNSAIDSが普通投与されるが、ひどい場合は、オピオイド投与も考慮される[22)]。

2.放射線皮膚炎

照射野に一致して生じ一般に治療開始から3週間ぐらいで生じるといわれている。物理的摩擦が生じるところに起きやすいといわれるため、患者にはきつい下着をつけない、入浴時に擦らないなどを指導し、場合によってはステロイド外用薬を処方する[1)]。びらん形成の際には非常に強い痛みを訴え食欲にも影響を与える。積極的な創傷処置と疼痛の管理が必要となる。皮膚炎は照射終了後1−2週間で消褪するが色素沈着が残ることもある。

3.放射線肺臓炎

照射野が肺にかかる場合問題となる有害事象に放射線肺臓炎がある。急性期の肺臓炎の症状は息切れ、咳、発熱を主たる症状とし、放射線治療後1ないし6か月で生じてくることが多いとされる。晩期障害として起きることが多いが照射中や照射終了後におこる場合もある。発熱、呼吸困難、咳などの症状が出現したときは速やかにCTで評価を行うのが重要である。照射野外に急速に

広がるときは重症化する場合が多くステロイドの投与が行われる。照射に伴い抗がん剤投与が行われることも多いので間質性肺炎の発症にも注意が必要である[19]。

4.口腔粘膜炎

抗がん剤もしくは放射線による粘膜の直接の障害によるもので、進展してびらん、潰瘍を生じると唾液分泌の低下も加わり局所の二次感染を起こすこともある。抗がん剤による口腔粘膜炎は口唇や頬粘膜、舌腹、口腔底など、角化の乏しい粘膜に生じやすく、放射線によるものは、照射部位に一致して生じる[23]。接触痛の改善にはステロイド軟膏が有効であり、ほかにキシロカイン咳嗽、アロプリノール咳嗽[19]、氷冷アルギン酸ナトリウム[24]などの効果が報告されている。

5.下痢

消化管へ照射された場合、急性毒性としての下痢を生じることがある[25]。感染性下痢との鑑別が重要だが否定できればロペラミド®などの止痢剤を投与するとともに脱水に対して十分な補液を行う。併用している抗がん剤によっても下痢は生じうるのでこの場合も対症療法を行うとともに重症度に合わせて薬剤の減量や中止を考慮しなければならない[26]。

術前放射線施行患者の栄養療法

術前に放射線療法を行うことは手術侵襲が加わる前であるため、術後と比して治療のコンプライアンスが高いという利点がある。食道癌や直腸癌では化学療法との併用で効果が報告されている。一方で、病巣の切除前であるため、原疾患由来の症状の継続や腫瘍増大抑制に乏しい場合もあるので、摂食不能、あるいは狭窄から閉塞状態になりうることも念頭に置かなければならない[27]。頭頸部癌や食道癌では治療前にすでに経口摂取が障害されている症例も多く、治療の経過中に経口摂取不可能になる症例もある。上述のような薬物療法を行い予防と治療を行うことが必要である。化学療法の副作用である消化管毒性については一時的であることが多いためまず経静脈栄養を行う。腫瘍による狭窄がある場合やまた放射線の影響による口腔粘膜障害や放射線食道炎が著明な場合は経鼻胃管による経腸栄養法やPEGの作成を考慮する。消化管内視鏡が通過しない症例では全身麻酔下小開腹で胃瘻を造設することも必要となることがある。上述した薬物治療を行うとともに経口摂取が不十分な患者においては栄養状態の悪化、耐術能の低下、術後の回復に影響を与える可能性があることも注意しなければならない。

術前の患者に栄養療法を行い、周術期の感染性合併症が減ることは多くの研究で明らかになっているため術前放射線療法を施行する前に栄養状態を評価し、必要なら栄養の介入を行うべきである。術前に化学療法や放射線療法を行うことの副作用による栄養障害を助長させない努力をすべきである。術前補助療法施行症例は術後も継続して栄養管理が必要である。NSTの稼働している施設では術前補助療法を開始する前にNSTの介入を始めるのが望ましい。

術前の栄養管理

2001年北欧諸国を中心にKehletらも含めたERAS study groupが組織され、結腸癌周術期管理のFast-track surgeryに関してERAS(Enhanced Recovery After Surgery) protocolとして推奨する22項目の対策が提唱されている。このプロトコールによって、それまで7日間であった結腸癌術後在院日数が3日まで短縮することができたとした報告[28]は注目を集め、同様の結果を得た報告が多くの施設から報告されるようになってきた。これら科学的根拠を集約することにより術後早期回復という目的に集約しており、栄養投与のみならず腸管機能促進と侵襲軽減の多様な介入は意義深い。この術後早期回復プログラムはmeta analysis[29]で有効性が確認されより広くの外科手術の分野でも採用され始めている。

ERASプロトコールの構成要素のうち特に栄養管理について

入院前の十分な情報提供および努力目標の確認と術前絶食の廃止、について言及されている。

入院前に十分な患者情報を収集するとともに入院の概要を説明する。その際栄養スクリーニングを行い栄養不良患者にはあらかじめ栄養管理計画を行い努力目標の一つとして確認することが重要である。周術期に放射線療法を施行する際には、施行前に栄養評価と栄養管理を行うことが必要とされる。

従来、全身麻酔で結腸癌の手術を受ける患者は、嘔吐や誤嚥を避ける意味で前日の夕食後、あるいは就寝以降絶飲食であることが多かった。諸外国のガイドラインでは飲水に関しては2-3時間、固形食物は6-8時間までとしているのが多い。特にERASプロトコールの中では濃度12.6%の炭水化物含有飲料であるNutricia PreOp®を手術前日に800mL、当日朝に400mLを引用することが推奨されているが日本では発売されていない。絶食により生じた飢餓により貯蔵炭水化物が消失するため、異化反応が惹起される。術前経口補液として炭水化物含有飲料を積極的に摂取することで、絶飲食による口渇感が軽減され不安感も解消されると言われている。また術後のインスリン耐性を減少させることが報告されており、耐糖能異常の軽減に役立つと考えられている。ESPENのガイドラインでは術前夜間からの絶食は必ずしも必要ではない(grade A)また術後栄養中断は必ずしも必要ではない(grade A)と記載されている。このプロトコルでも感染性合併症を回避するために術後早期からの経口、あるいは経腸栄養が推奨されており、そのために腸管機能の回復のために過剰な輸液を回避することと、嘔気嘔吐の予防策を講じることが推奨されている。ただし、消化器疾患、とくに通過障害がある場合や胃排泄遅延があるとき、救急疾患は除外すべきであり、症例の状態を考慮すべきであると考える。

わが国では2012年7月に日本麻酔科学会が術前絶飲食ガイドライン(表1)をWEB上で公表している。清澄水の摂取は麻酔導入2時間前まで安全であり(推奨度A)、麻酔全2-3時間までの清澄水摂取により患者の口渇感が減少し、快適度が増すなどの利点が示されている。

表1 公益財団法人日本麻酔科学会 術前絶飲食ガイドライン2012年7月

摂取物	絶飲時間
清澄水	2時間
母乳	4時間
人工乳・牛乳	6時間

表2 術前絶飲食ASAガイドライン(ASA:アメリカ麻酔学会)

摂取物	絶飲時間
清澄な液体(水、繊維物を含まないジュース、茶、炭酸飲料、コーヒー)	2時間
母乳	4時間
粉ミルク	6時間
牛乳	6時間
軽食(脂肪や肉を含まない)	6時間
常食	8時間

摂取量については10mL/kgあるいは無制限を採用しており飲める範囲での摂取は可と考えられている。母乳の摂取は4時間まで安全である(推奨度C)が人工乳・牛乳の摂取は6時間まで安全である(推奨度C)。軽食については欧米のガイドライン(表2)で摂取から麻酔導入まで6時間以上開けること、揚げ物、脂質を多く含む食物、肉の場合は8時間以上空ける必要がある。術前の絶飲食は主に胃液誤嚥を防ぐために行われていて、pHが2.5以下あるいは25mL以上の胃液を誤嚥した場合誤嚥性肺炎のリスクが高いといわれている。お茶などの清澄な液体は1時間で95%が排泄されるため、2時間の絶飲後の胃液の基礎分泌量と唾液嚥下量を反映する。乳児から成人までの待機手術患者において、麻酔導入2-3時間前までの清澄水摂取が胃内溶液に与える影響は不変あるいは減少し、胃内溶液pHに与える影響は不変であった。またいずれの研究においても絶飲時間と嘔吐、逆流、あるいは誤嚥発生率の関連性は検討されていないが、胃内容液量と胃内容液pHの所見から、誤嚥の危険性は増加しないことを示している。

術中栄養療法

術中は術前からの飢餓や手術侵襲によって、脂質やタンパク質が分解される異化が生じる。ブドウ糖の術中投与によるタンパク保持効果を検証したRCTがあり[30]、タンパク異化反応を抑制し血糖値を上昇させた。このようにタンパク異化反応を抑制する可能性があるが、血糖値は上昇しやすく術後感染症などを改善するか否かについては今後の検証が必要である。

まとめ

癌の治療成績やQOLの向上のため周術期に放射線照射などの補助療法が施行されるようになってきている。治療前の早期からの栄養評価と栄養介入を行うことと、周術期の絶飲食期間をなるべく短縮し、栄養投与のみならず、腸管機能の回復と侵襲の軽減に努めることが重要である。周術期に行われる放射線療法の影響を十分考慮し、的確な栄養管理の計画と実行が必要とされている。

参考文献

1) 師田まどか，小口正彦．知っておきたいがん放射線治療の知識 放射線治療の実際 外科治療 99(4)：395-402，2008.
2) Luu, T. D., P. Gaur, Force, S. D.et al.. "Neoadjuvant chemoradiation versus chemotherapy for patients undergoing esophagectomy for esophageal cancer." Ann Thorac Surg 85(4) : 1217-1223; discussion 1223-1214, 2008.
3) Reynolds, J. V., N. Ravi, Hollywood, D. et al. (2006) . "Neoadjuvant chemoradiation may increase the risk of respiratory complications and sepsis after transthoracic esophagectomy." J Thorac Cardiovasc Surg 132(3) : 549-555, 2006.
4) 田村茂行，岡田かおる，三木宏文ほか．臓器別に学ぶがんの知識・治療・栄養療法 頭頸部がん、Nutrition Care 2(4)：360-365，2009.
5) 中島寅彦．頭頸部癌に対する化学放射線療法の元凶と将来展望．日気食会報、62(2)：241-242，2011.
6) Iizuka, T., H. Ide, Kakegawa, T., et al. "Preoperative radioactive therapy for esophageal carcinoma. Randomized evaluation trial in eight institutions." Chest 93(5) : 1054-1058, 1988.
7) de Manzoni, G., C. Pedrazzani, Laterza, E., et al. "Induction chemoradiotherapy for squamous cell carcinoma of the thoracic esophagus: impact of increased dosage on long-term results." Ann Thorac Surg 80(4) : 1176-1183, 2005.
8) Morgan, M. A., W. G. Lewis, Hopper, A. N., et al.. "Prospective comparison of transthoracic versus transhiatal esophagectomy following neoadjuvant therapy for esophageal cancer." Dis Esophagus 20(3) : 225-231, 2007.
9) Gebski, V., B. Burmeister, Smithers, B. M. et al. "Survival benefits from neoadjuvant chemoradiotherapy or chemotherapy in oesophageal carcinoma: a meta-analysis." Lancet Oncol 8(3) : 226-234, 2007.
10) van Hagen, P., M. C. Hulshof, van Lanschot, J. J. et al. "Preoperative chemoradiotherapy for esophageal or junctional cancer." N Engl J Med 366(22) : 2074-2084, 2012.
11) 根本建二．食道癌に対する化学放射線療法．週刊医学のあゆみ 227(9)：714-718，2008.
12) Tachimori, Y., N. Kanamori, Uemura, N. et al. "Salvage esophagectomy after high-dose chemoradiotherapy for esophageal squamous cell carcinoma." J Thorac Cardiovasc Surg 137(1) : 49-54, 2009.
13) Swisher, S. G., P. Wynn, Matthews, B, et al. "Salvage esophagectomy for recurrent tumors after definitive chemotherapy and radiotherapy." J Thorac Cardiovasc Surg 123(1) : 175-183, 2002.
14) Dobie, S. A., J. L. Warren, Matthews, B. et al. (2008) . "Survival benefits and trends in use of adjuvant therapy among elderly stage II and III rectal cancer patients in the general population." Cancer 112(4) : 789-799, 2008.
15) Mohiuddin, M., K. Winter, et al. "Randomized phase II study of neoadjuvant combined-modality chemoradiation for distal rectal cancer: Radiation Therapy Oncology Group Trial 0012." J Clin Oncol 24(4) : 650-655, 2006.
16) Crane, C. H., J. M. Skibber, Feig, B. W, et al.. "Response to preoperative chemoradiation increases the use of sphincter-preserving surgery in patients with locally advanced low rectal carcinoma." Cancer 97(2) : 517-524, 2003.

17) Bosset, J. F., L. Collette, et al. "Chemotherapy with preoperative radiotherapy in rectal cancer." N Engl J Med 355(11) : 1114-1123, 2006.
18) Sauer, R., H. Becker, Hohenberger, W., et al. "Preoperative versus postoperative chemoradiotherapy for rectal cancer." N Engl J Med 351(17) : 1731-1740, 2004.
19) 宮崎達也，宗田真，田中成岳ほか．食道癌放射線化学療法の有害事象とその対策．消化器外科 33：1333-1338，2010.
20) 桑和田昇，放射線食道炎の臨床的研究，鹿児島大学医学雑誌32：281-307，1980.
21) 小川真一，野村邦紀，野口京ほか．頸部食道癌の化学放射線療法による急性粘膜炎に対する和漢薬治療の効果：予備的経験．日放腫会誌 19：41-44，2007.
22) 雨田貞幹．化学放射線治療中の患者に対する痺痛管理法．癌の臨床 57(2)：2011.
23) 岸本裕充．急性期病院における口腔管理．兵医大医会誌（Acta Med. Hyogo.） 37(1)：43-50，2012.
24) 竹山美也子，川上恵以子，栁川のり子ほか．アルロイドGアイスボール内服による放射線食道炎の疼痛軽減．第37回成人看護Ⅱ：247-249，2006.
25) 小口正彦，小塚拓洋，室伏景子ほか．直腸がんの放射線治療．消化器外科 NURSING 15(11)：64-71，2010.
26) 佐藤温．下痢．大村健二編．癌患者の栄養管理．南山堂，東京，2009.
27) 中野徹．術前化学療法中の栄養管理．大村健二編．癌患者の栄養管理．南山堂，東京，2009.
28) Ljungqvist, O. and E. Soreide, "Preoperative fasting." Br J Surg 90(4) : 400-406, 2003.
29) Fearon, K. C., O. Ljungqvist, et al. "Enhanced recovery after surgery: a consensus review of clinical care for patients undergoing colonic resection." Clin Nutr 24(3) : 466-477, 2005.
30) Schricker, T., R. Lattermann, et al. "Intraoperative protein sparing with glucose." J Appl Physiol 99(3) : 898-901, 2005.